EXPERIMENTS WITH PURE ELECTRON PLASMAS

J. H. Malmberg, C. F. Driscoll, B. Beck, D. L. Eggleston,*
J. Fajans, K. Fine, X.-P. Huang, and A. W. Hyatt**
Department of Physics
University of California at San Diego, La Jolla, CA 92093

ABSTRACT

A series of experiments at UCSD on pure electron plasmas is described. The apparatus and methods of measurement are discussed. Results are given on various wave experiments including the dispersion of electron plasma waves, feedback growth and damping of the $l = 1$ diocotron wave, and the unstable growth of diocotron waves on plasmas with hollow radial profiles. The nonlinear saturation of diocotron waves, subsequent vortex merging and the decay of the resulting two-dimensional turbulence are observed. Transport processes resulting from both the single particle and collective response of the plasma to externally imposed field asymmetries have been studied. Evolution of the confined plasma to thermal equilibrium has been observed and scaling of the rate of this evolution with magnetic field has been measured. The relaxation rate of an anisotropic velocity distribution has been measured in both the usual parameter regime and the cryogenic regime where the rate is greatly reduced due to the existence of a many particle adiabatic invariant.

I. INTRODUCTION

In recent years the plasma group at UCSD has been studying the properties of plasmas for which all particles have the same sign of charge, specifically plasmas composed entirely of electrons. These plasmas are unusually simple both experimentally and theoretically but they nevertheless exhibit a wide range of collective and statistical mechanical effects. In this lecture I will describe some of the experiments we have performed with this system. Since a number of the other groups interested in the field will present papers at this symposium I will restrict my presentation to the UCSD work, and it should not be inferred that this is intended as a scholarly review of the field. Instead this paper is tutorial in nature and on the work of a single group. Since Tom O'Neil has just given a survey of the theory I will confine most of my discussion to the experiments.

---

*Present address: Physics Dept., Occidental College, Los Angeles, CA 90041
**Present address: General Atomic, P.O. Box 85608, San Diego, CA 92138

Our interest is plasma physics; and it is primarily that interest, not differences in containment geometry, that distinguishes the UCSD work from the large body of elegant research on small numbers of particles in traps. The long-term goal of our research is to obtain a deep and detailed understanding of various plasma phenomena in the simplest cases that we are able to devise. We hope that this research will produce a set of paradigms which will be useful for understanding the more complex behavior typical of most laboratory and naturally occurring plasmas.

The series of experiments at UCSD has shown how to make and contain nonneutral electron plasmas by simple methods, and has permitted precision measurements of their wave and transport properties. The magnetized column of electron gas is a plasma by the criterion that the Debye length is small compared to the radius of the column. Except for a slow rotation, the plasma is at rest in the laboratory frame of reference. This fact distinguishes these plasmas from those obtained in electron beam experiments; for experiments this distinction is crucial. Wall interactions and collisions with impurity or background neutrals are negligible effects in the pure electron plasma, so the dynamical evolution is governed by plasma physics and is not complicated by atomic and surface physics.

Nonneutral plasmas are unique in that conservation of total canonical angular momentum provides a constraint on the allowed radial positions of the particles: if no external torques act on the plasma, the plasma cannot expand to the walls. Internal interactions among the particles will then drive the plasma towards a confined thermal equilibrium state. The existence of magnetically confined thermal equilibrium states is a unique and important property of nonneutral plasmas. Eventually, effects which break cylindrical symmetry slowly transfer angular momentum to the plasma, and the particles are slowly lost to the wall.

Another property of pure electron plasmas is that recombination cannot occur even if the temperature is lowered towards absolute zero, since there are essentially no ions in the containment volume. As the plasma temperature is reduced, electron-electron correlations become strong. This puts the plasma into a previously unexplored parameter range. At sufficiently low temperatures and sufficiently high densities, theory predicts that the electron gas will liquify, and that at still more extreme conditions, it will freeze into a crystal.

A major thrust of our research is to use the pure electron plasma with conventional parameters as a model system to study transport. The electron plasma displays in some form many of the transport effects thought to be important in neutralized plasmas, but it is a substantially simpler system. The low-noise, repeatable pure electron plasma is also excellent for various wave experiments.

The pure electron plasma can be manipulated by a number of experimental techniques. These include axial compression and stacking, radial compression by magnetic field ramping, and heating by voltages

applied to the axial containment electrodes. These techniques are used routinely in our devices and may be useful to others in manipulating plasma particles in their traps.

In this lecture, I will describe the apparatus and measurement techniques and then turn to some of our experimental results on waves and transport.

II. EXPERIMENTAL DEVICES AND TECHNIQUES

The electron plasma is contained in cylindrical geometry, with an axial magnetic field providing radial confinement, and applied potentials providing axial confinement. The containment apparatus is shown schematically in Figure (1). The entire apparatus is immersed in a uniform static axial magnetic field. The boundary conditions on the electrostatic field are determined by a conducting wall; the wall consists of a series of electrically isolated cylinders of various lengths [for simplicity, only three are shown in Figure (1)]. Any of these cylinders can be biased sufficiently negative to contain the plasma axially. Some wall cylinders are divided into angular sectors which can be used to launch or detect waves having azimuthal dependence $e^{il\theta}$.

The source of the electrons is a directly heated spiral of tungsten wire. The center of this spiral is biased negatively with respect to ground. The space charge potential of the plasma closely matches the filament potential.[1–4] The overall filament bias voltage then determines the line density of electrons N (number/cm length), while the ohmic potential drop across the filament determines the number density n (number/cm^3). These potentials are chosen to obtain the desired experimental parameters. The approximately parabolic radial potential across the filament due to the ohmic potential drop is the boundary condition that allows us to inject a *plasma*, i.e. a collection of charges with radial size large compared to the Debye length.

Several experimental apparatuses have been built. For one class of machines the containment electrodes are at room temperature. We are presently operating two of these apparatuses, denoted V′ and EV. The neutral pressure is $\leq 10^{-10}$ Torr with $B \leq 700$G. Typically the plasma density is 10^7 cm^3 and the plasma temperature is 1 eV. These apparatuses are mainly used to study waves and transport processes. The cryogenic apparatus (CV) is based on a superconducting magnet, to obtain fields of 80 kG and pressures in the 10^{-14} Torr range, with the containment portion of the apparatus at 4.2 °K. Typically the plasma density is $\leq 4 \times 10^{10}$ cm^3 and the temperature is 6 °K $\leq T \leq 2 \times 10^7$ °K. On the cryogenic apparatus, the filament has been moved axially into a lower magnetic field region, giving substantially different injection characteristics.[5] This apparatus is designed to study plasma properties in the rather unusual regime of high field and low temperatures, including the correlated liquid state.[6,7]

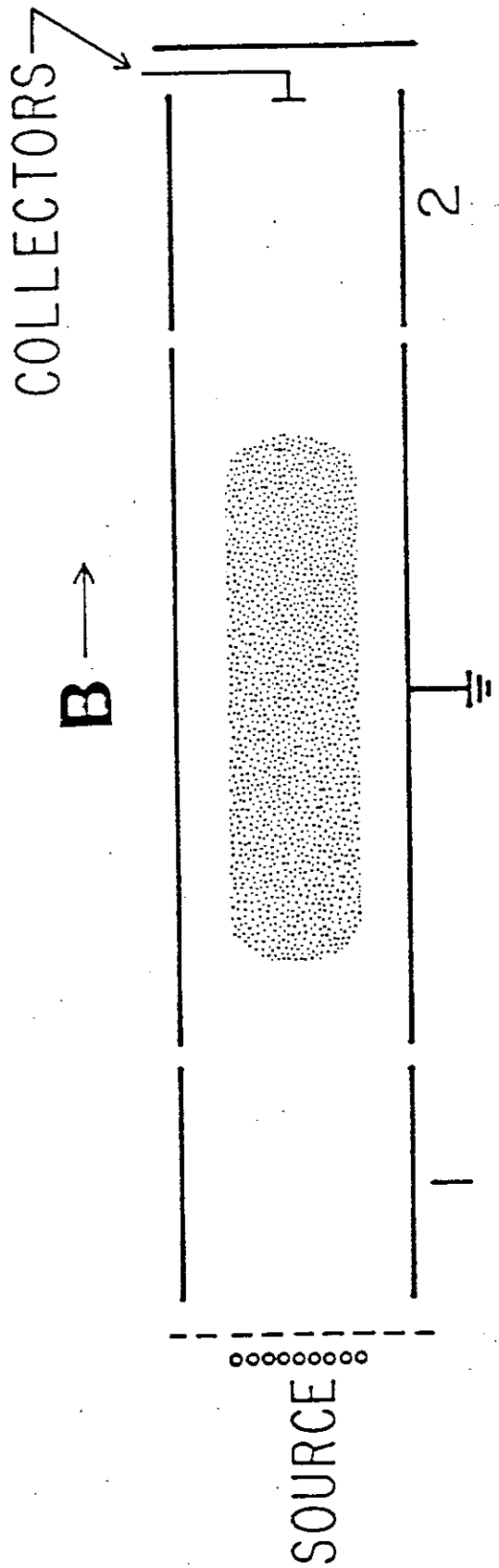

Figure 1. Schematic of the containment apparatus.

The systems normally operate in an inject, hold, dump/measure cycle. During injection, all wall cylinders are grounded except for a dump gate (e.g. #2 in Figure 1) which is biased negatively, giving a column of electrons between the filament and this gate. A portion of this plasma column is trapped by gating a second cylinder (e.g. #1) negative. This gives a trapped plasma column. The length of the column is variable since in the real apparatus there are many cylinders and thus many choices for the injection and dump gates. Since the axial containment is energetically assured, the electrons can be lost only by radial transport across the magnetic field to the cylinder walls. The plasma column is rotating, since the radial electric field due to space charge gives an $\mathbf{E}\times\mathbf{B}$ drift in the $\hat{\theta}$ direction. The electron plasma contains a negligible number of positive ions, since ions are not confined longitudinally.

After a variable containment time, the dump gate is pulsed to ground potential, allowing the remaining electrons to stream out axially along the field lines for collection and analysis. The injection/hold/dump cycle may be repeated up to 60 times per second with nearly identical injection conditions, allowing the time evolution of the plasma to be constructed from many separate measurements with differing containment times.

The collection electrodes include end plates in various geometries for collecting the remaining electrons, and may include a small movable collector for measuring the electrons remaining on the field line at a particular (r,θ). We also analyze the electrons as they are dumped to obtain the thermal energies $T_\parallel$ and $T_\perp$ characterizing the plasma. $T_\parallel$ is obtained by measuring the number of electrons which are energetic enough to escape axially as the containment voltage on the dump gate, V_c, is slowly made less negative. For a Maxwellian particle distribution, the first charge collected varies approximately as $Q \approx \exp(\alpha e V_c / T_\parallel)$, where $\alpha \approx 1$. We have developed this method thoroughly, including the effects of space-charge and plasma expansion during the analysis process.[8,9] To obtain $T_\perp$, a beam of exiting electrons is allowed to pass through a small hole in the end plate. An electrostatic velocity analyzer measures the change in the parallel energy of these electrons caused by a secondary magnetic field.[8,10,11] Since the magnetic moment for each electron is conserved, the average parallel energy changes by $\Delta E_\parallel = -(\delta B/B)T_\perp$. With this method, we routinely obtain $T_\perp$ at all radii to a few percent accuracy.

Techniques for longitudinal compression and "stacking" of nonneutral plasmas have been developed.[5] The containment cylinders are electrically divided into many sections, so it is possible to slowly or abruptly change the applied potential on part of the wall, thereby compressing or expanding the plasma longitudinally. With proper sequencing of wall potentials, we can "stack" plasmas by repeatedly trapping new batches of electrons in a cylinder near the injector and then adding them to the main plasma in a different section. These techniques allow us to easily manipulate the plasma density, and to heat or cool the plasma. The plasma density and radius can

also be modified by magnetic field "ramping" -- i.e., increasing or decreasing the magnetic field after the plasma has been captured. Of course, magnetic manipulations necessarily proceed slower because the inductive time scale ranges from tenths of seconds on V′ and EV to hundreds of seconds on CV.

III. WAVES

Electron Plasma Waves

Nonneutral plasmas exhibit many of the same collective phenomena as neutral plasmas. The dispersion relation for electron plasma waves in an infinitely long nonneutral plasma is the same as it is in a neutral plasma, except for the Doppler shift due to the $E \times B$ rotation of the nonneutral plasma.[1,4,12,13,14] These waves can be launched and detected by electrically isolated sections of the cylindrical wall (sector probes), which give a signal due to image charge fluctuations.[15] Electron plasma waves exhibit essentially 100% reflection at the ends of the plasma column. Thus as a transmitter is swept there is a series of resonances at frequencies which produce standing waves. The sectors at various angles can be connected to transmit and receive only $l = $odd or $l = $even waves. A typical transmission spectrum for $l = $odd plasma waves is given in Figure 2.

An experimentally measured dispersion relation for the $l = 0$ electron plasma wave is shown in Figure 3. The dots are experimental points and the line is the theory. This dispersion relation is already well known from neutral plasma experiments. The wave frequency decreases at longer wave lengths because of finite size effects.[16,17] Similar, but doppler shifted, dispersion relations are obtained for angularly dependent modes with $l = \pm 1$. It should be noted that the $l = \pm 1$ angular directions are not physically identical since the plasma is spinning. Prasad and O'Neil[18] make a corresponding distinction between the "plasma" and "diocotron" branches of the dispersion relation.

In one sense, waves are well understood in these trapped plasmas, but in another sense they are not. Typically, we find excellent agreement with theory for the real part of the frequencies, and for growth and damping rates which are determined by fluid theory. However, effects such as Landau damping, which depend on the details of the velocity distribution at a wave-particle resonance are not usually in agreement with simple models. The plasma is trapped, and a mode can act over a long time to produce a plateau (or trapped particle distribution) in the resonant velocity region. The electrons are confined and have a comparatively low collision rate. Under these circumstances it is comparatively easy for wave phenomena to produce substantial nonlinear distortions in the distribution function of the electrons, thereby confusing efforts to make linear measurements.

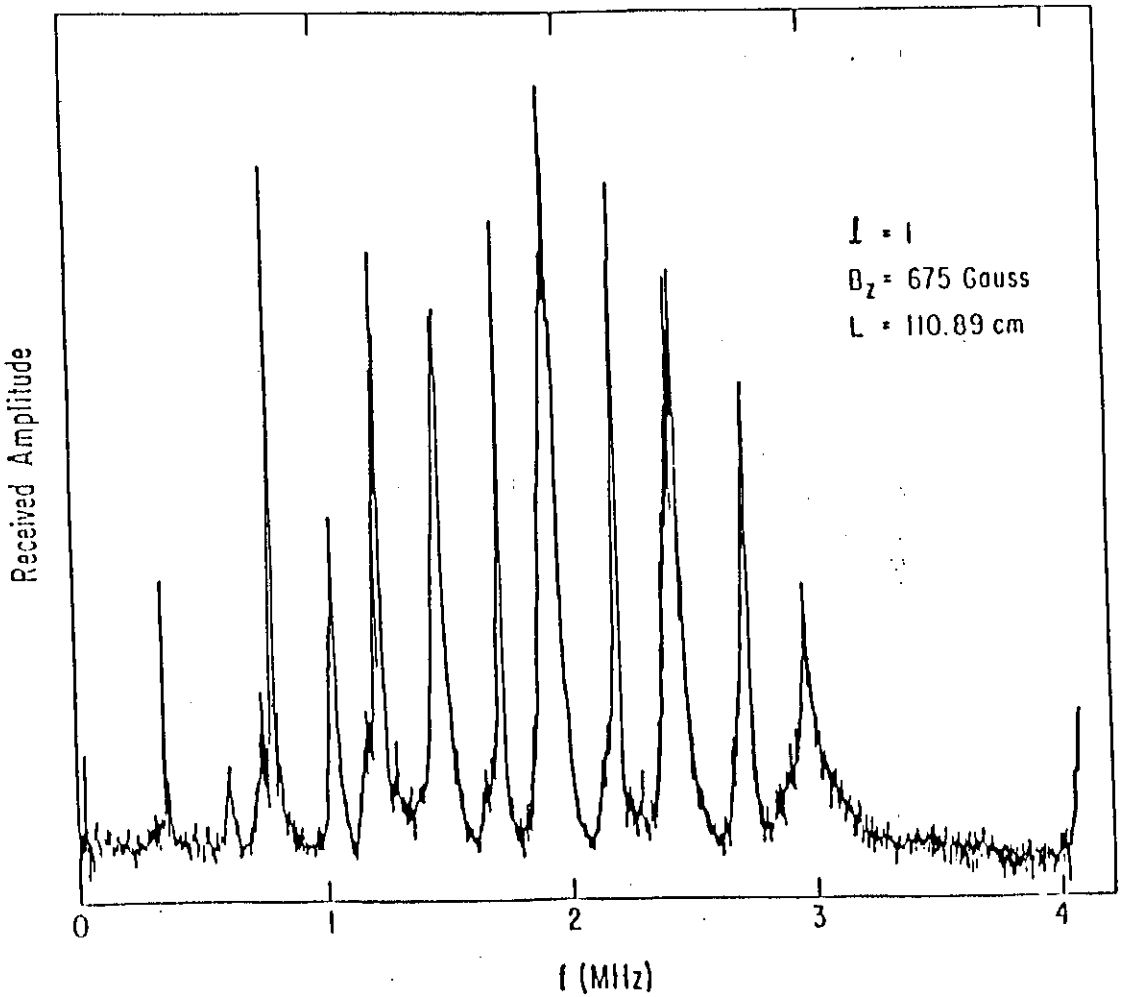

Figure 2. Transmission spectrum for ℓ = odd electron plasma waves.

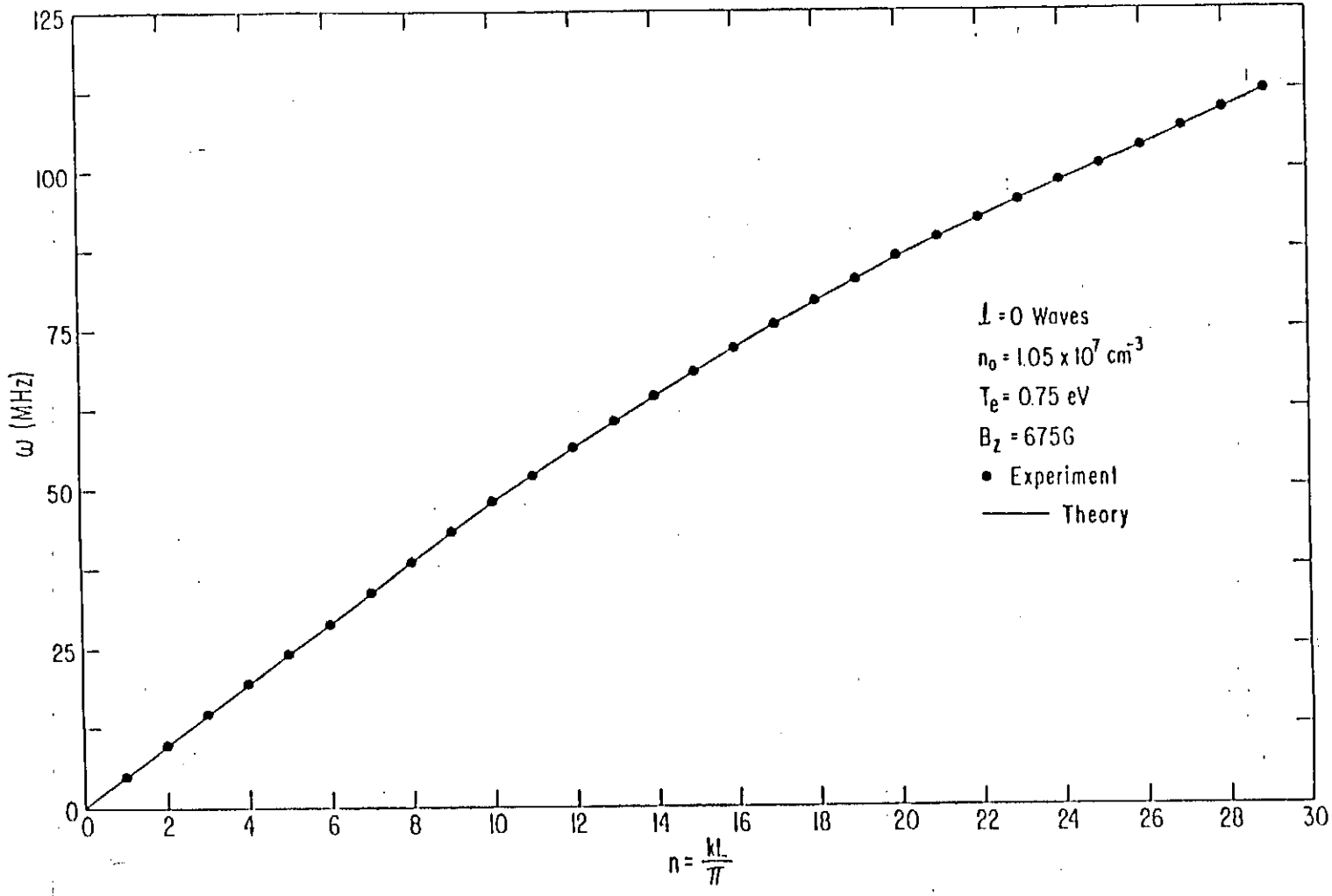

Figure 3. Dispersion relation for $\ell = 0$ electron plasma wave.

Diocotron Waves

We have also measured properties of those diocotron waves which have $k_z \simeq 0$[12,19–22] and an angular dependence $e^{il\theta}$. The waves arise because an essentially two-dimensional perturbation of the plasma density results in an electric field, which causes an $\mathbf{E}\times\mathbf{B}$ drift of the plasma, which in turns self-consistently generates the density perturbation. Waves with angular dependence $l = 1,2,3$ have been unambiguously identified and studied.

If the plasma density is monotone decreasing in r and the wall is a perfect conductor, the diocotron waves are stable. Typically, for $l \geq 2$ electrons at some radius are drifting around the axis in resonance with the wave and the modes are heavily damped by a Landau-like process.[22] The $l = 1$ mode is undamped because only electrons right at the wall would be resonant with the wave and there are no particles at that radius. Experimentally, we observe essentially no change in the $l = 1$ wave amplitude over a time of several seconds (i.e. $\sim 10^5$ cycles).

Figure 4 shows a cartoon of an $l = 1$ diocotron wave in cross section. Small amplitude wave theory predicts that the $l = 1$ diocotron wave perturbation is a rigid displacement of the electron column off the central axis of the containment cylinder. The electric field due to the asymmetric image charge on the wall makes the electron column rotate about the containment axis at the wave frequency, while also rotating about its own center at a higher frequency. We find experimentally that this characterization of the density perturbation as a displacement off axis is valid up to very large wave amplitudes. It is more instructive to call this phenomena a dynamical equilibrium than a mode. It is the most ubiquitous motion of the plasma and is essentially undamped. An exactly centered plasma should be considered just a special case in the continuum of possible offsets.

The $k_z = 0$ diocotron waves are negative energy modes and can be destabilized by wall resistance. It is apparent from Figure 4 that as the plasma shifts off-center, electrostatic energy decreases, so it is intuitively obvious that this mode has negative energy. If an isolated section of the wall is connected to the rest of the wall by a resistor as shown, then as the column of plasma drifts about the machine axis image charges flow back and forth through the resistor and dissipate energy. Since the mode has negative energy, this dissipation of energy makes the mode grow.[23] This effect is shown in Figure 5. Initially there is a neutrally stable, $l = 1$, $k_z = 0$, diocotron mode at small amplitude. Unshorting the resistance to the wall sector destabilizes the wave and it grows by 30 db. At 30 ms the resistor is shorted and the large amplitude wave is again almost neutrally stable (the slight growth is due to a 50 ohm amplifier impedance connected to another wall sector). The observed growth rate as a function of resistance, distributed capacity, magnetic field and plasma density are all in good agreement with a perturbation theory which considers the wall impedance to

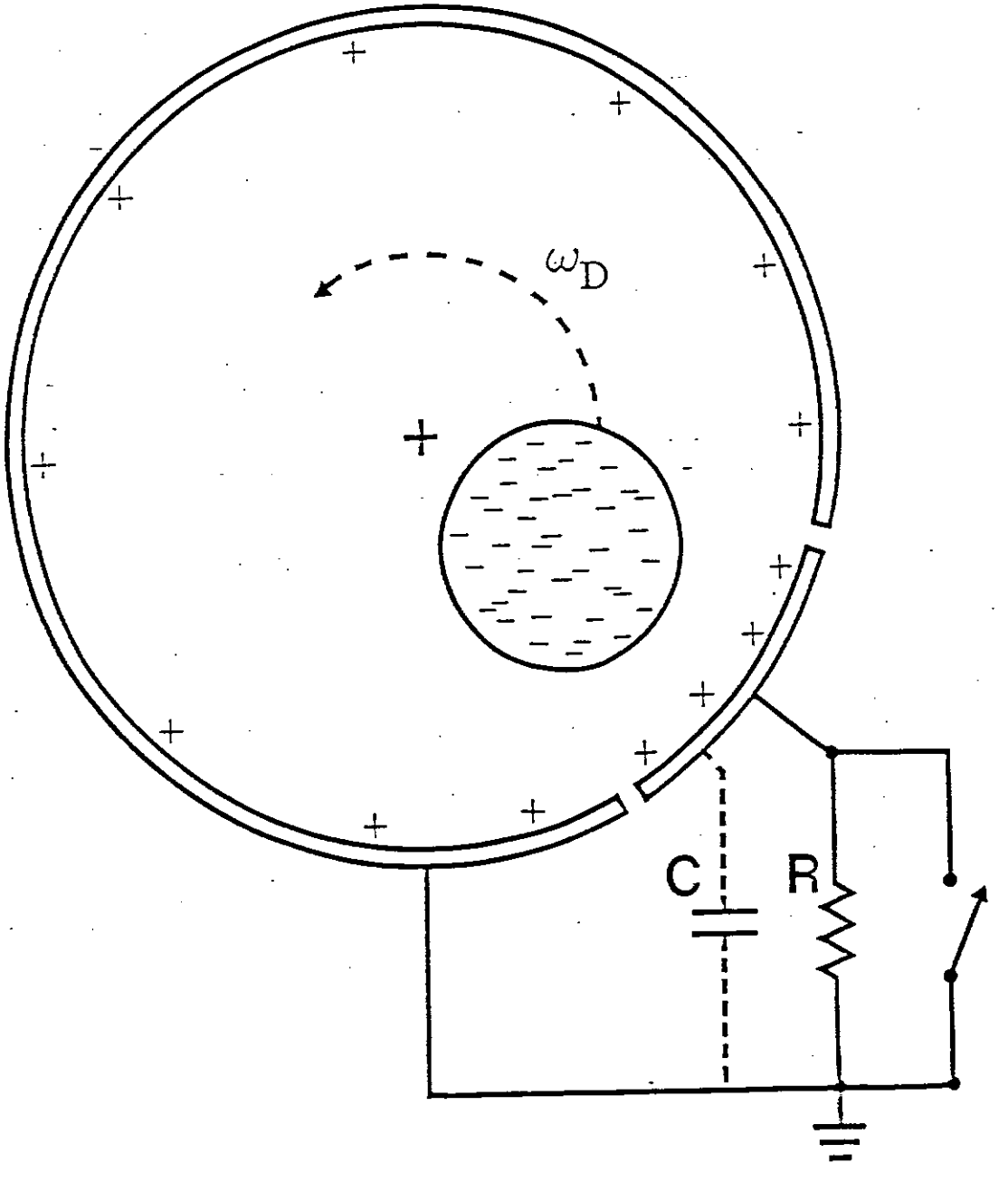

Figure 4. Cartoon of an $\ell = 1$ diocotron wave.

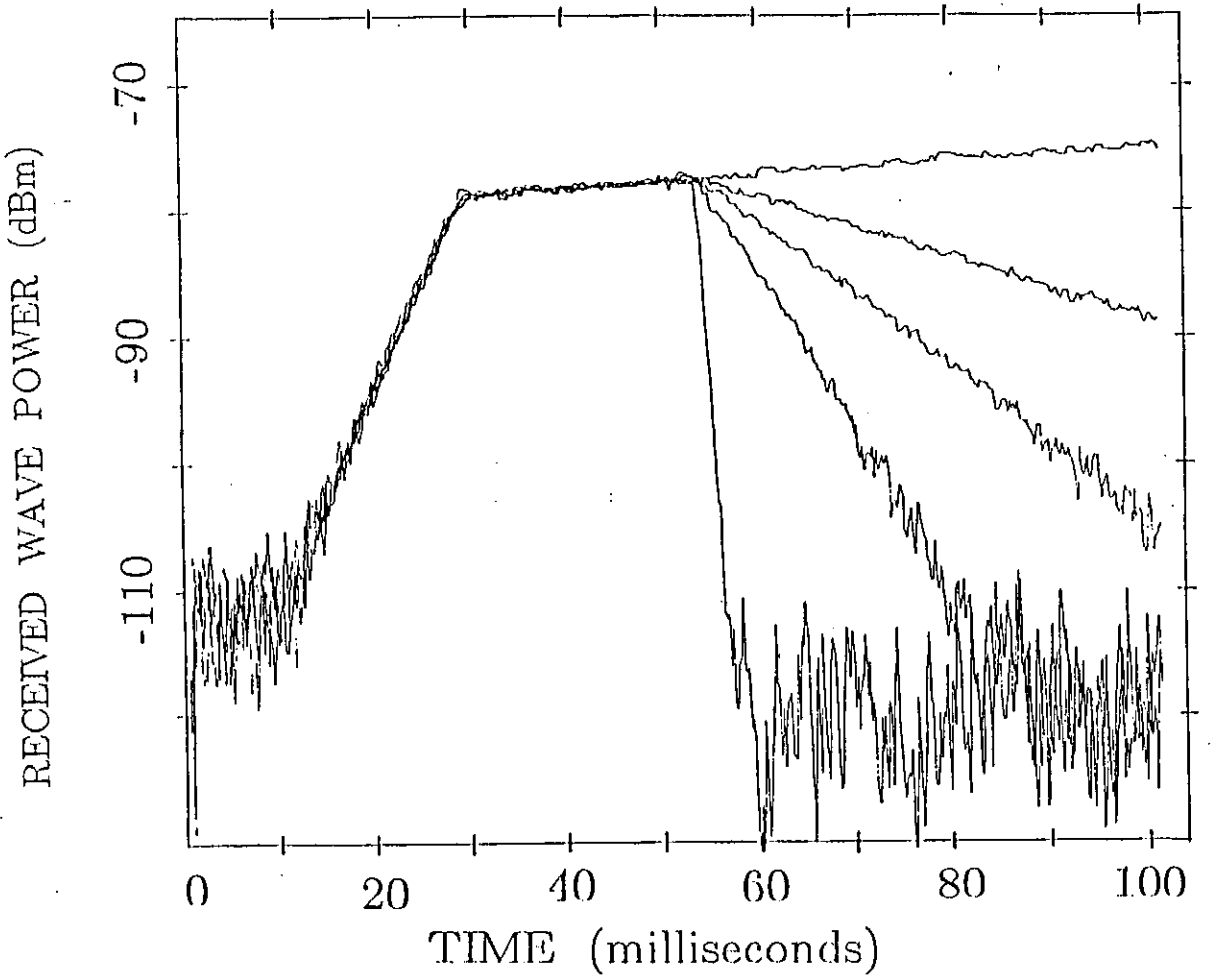

Figure 5. Resistive growth and feedback damping of an $\ell = 1$ diocotron mode.

be a boundary condition on the wave.[23]

The damping beginning at 53 ms is the result of feedback.[24] The wave signal is received on one wall sector, amplified with proper gain and phase shift, and fed back to a second sector. The second sector delivers power to the wave and causes it to damp at a rate depending on amplifier gain. We have measured the damping rates due to various gains, phases, and sector placements, and find good agreement with theory.

The two dimensional density perturbation $n(r,\theta,t)$ associated with the wave has been measured by dumping the plasma synchronous with the wave phase[25], and thereby measuring the number of electrons at a particular $(r,\theta-\omega t)$. A typical result is shown in Figure 6 for two different wave amplitudes. At large amplitudes the column shape becomes elliptical with the elongation in the θ-direction. The shape distortion and amplitude dependent shifts in frequency are in excellent agreement with a waterbag computer code.[25] The code iterates both the frequency and plasma shape until the plasma boundary is coincident with an effective potential contour in a frame rotating at the $l=1$ frequency. The wave evolution of Figure 5 thus corresponds to shifting the electron column off axis part way to the wall, then shifting it back to the axis. To lowest order there is no change in the radial profile induced by this process.

Diocotron Instabilities

If the radial density profile is hollow instead of monotone decreasing in r, then for long plasmas a set of unstable diocotron modes which are driven by the shear in the rotational drift velocities is observed.[26] The perturbed eigenmodes of these unstable waves are mostly on the inside of the plasma column. They coexist with the stable modes: the perturbed density of the stable modes peaks on the outside. The unstable modes are the nonneutral plasma analogue of the Kelvin-Helmholtz instability: they are the "diocotron instability" that decades ago was observed to break up hollow electron beams.[27-29] These $k_z=0$ instabilities are observed for a wide range of initial density profiles, from barely non-monotonic to fully hollow shells. Using the synchronizing method previously described, we measure the z-averaged density $n(r,\theta,t)$ and the temperature $T(r,t)$. From the data we can extract both the time evolution and the eigenfunction $\delta n_l(r,t)$ of the various modes in the plasma.

We have observed a new non-exponential instability with azimuthal mode number $l=1$ coexisting with the stable $l=1$ diocotron mode.[26] This new unstable mode has been overlooked by prior theory, but is predicted by a new theory developed by Rosenbluth and his collaborators.[30] It is growing more slowly than exponentially, but it can nevertheless dominate the plasma evolution.

We also obtain accurate growth rates for an exponentially unstable $l=2$ mode coexisting with the stable $l=2$ mode. These modes are not

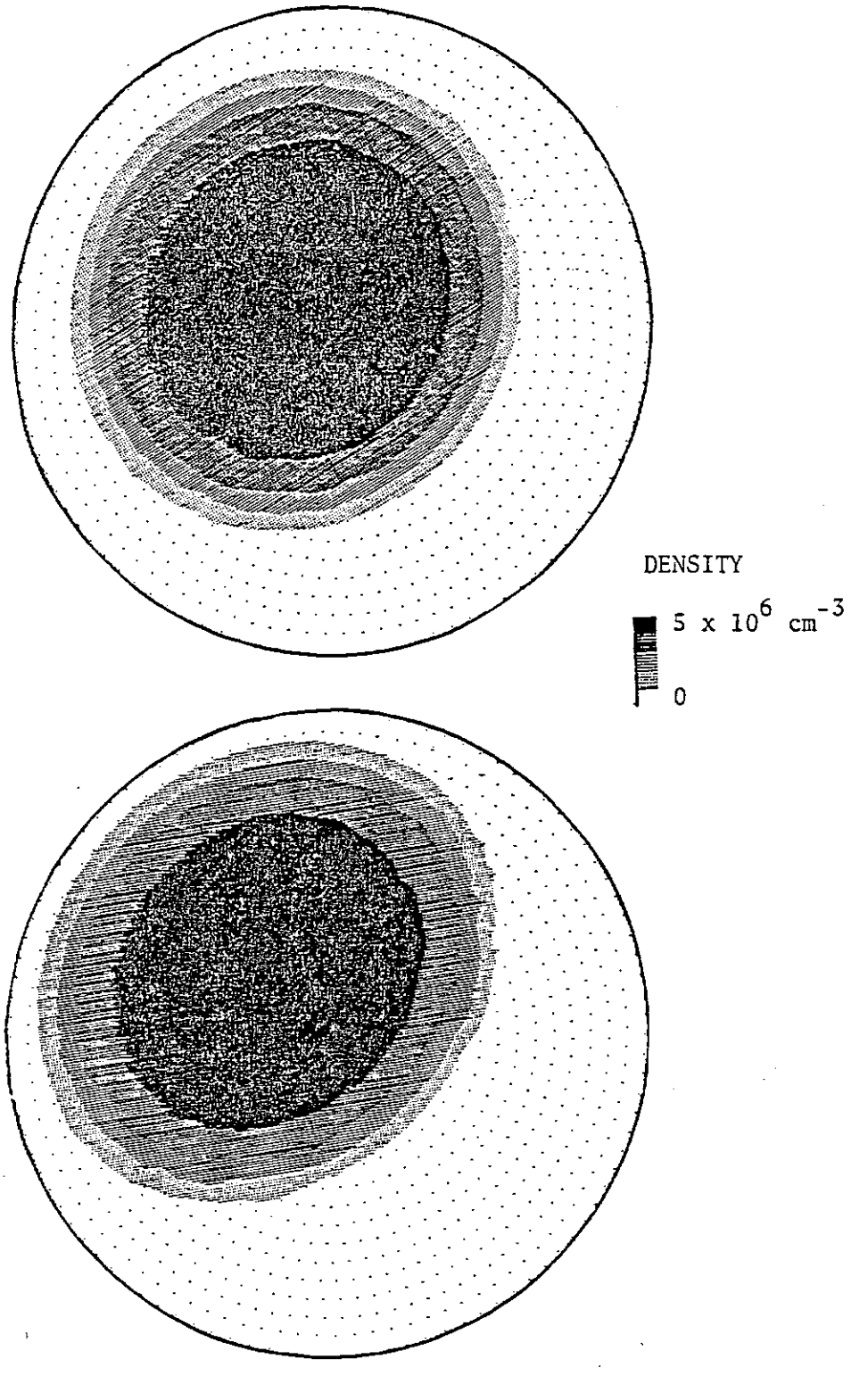

Figure 6. Two dimensional density associated with an $\ell = 1$ diocotron wave. The outer circle is the location of the conducting wall.

complex conjugate pairs as one would expect from simple calculations for step-function density profiles.[12] However, the real parts of frequencies agree well with numerical calculations of dispersion relations for realistic profiles.[26,30] For $l=2$, the measured growth rates and eigenfunctions are in "factor-of-two" agreement with the predictions of two dimensional drift theory.

We have experimentally investigated the large scale cross field transport associated with these instabilities, which is much faster than collisional transport.[31] This transport proceeds until the plasma has a monotone decreasing radial density profile and is no longer unstable. This effect is shown in Figure 7 which gives radial profiles taken at a series of times. At $t=0$, some electrons are allowed to escape from the center of a quiet plasma to produce the hollow profile shown. At 100 μsec the profile is beginning to exhibit increased shot-to-shot noise. Each of the horizontal lines represents an individual measurement at that particular radius. By 200 μsec the shot-to-shot noise is very large and the hollow in the center is gone. After 2 milliseconds, the plasma density is peaked in the center and most of the noise is gone.

We can understand this evolution geometrically by synchronizing the plasma dump to the fastest growing unstable wave to produce two dimensional plots of the plasma density at various times. An example of the result is given in Figure 8. (This case is similar but not identical to the case in Figure 7.) The initial plasma has a central density about 50% of the edge density, giving an $\mathbf{E}\times\mathbf{B}$ drift profile with strong rotational shears. This plasma is quite symmetric in the θ direction, except for a very small seed wave with azimuthal mode number $l=2$, which is the fastest growing mode. At a time 1 μsesc after the plasma has been hollowed, the seed wave is barely noticeable. The seed wave grows exponentially on a time scale of 30 μsec until it saturates with the formation of two nonlinear vortex structures, seen in the plot at 110 μsec. These vortices rotate about each other and about their own centers, until they merge (160 μsec) and form chaotic density variations on smaller spatial scales. The resulting 20% noise fluctuations decay on a time scale of several hundred microseconds, leaving a monotonically decreasing plasma density at 1000 μsec. Thus this instability undergoes nonlinear saturation with the formation of vortices, then the vortices decay into turbulent noise, and finally the noise decays leaving a reasonably quiet quasi-equilibrium. The collisional transport to thermal equilibrium then occurs on a time scale about 10^4 times longer. This separation of time scales allows the study of collisional transport to thermal equilibrium uncontaminated by instability effects.

The instability and merger of the vortex states may be of fundamental interest. Since the initial conditions can be accurately controlled and the system has low noise, the vortex dynamics can be studied precisely. Although point vortex approximations have been studied for some time, only recently has theoretical progress been made on the dynamics of

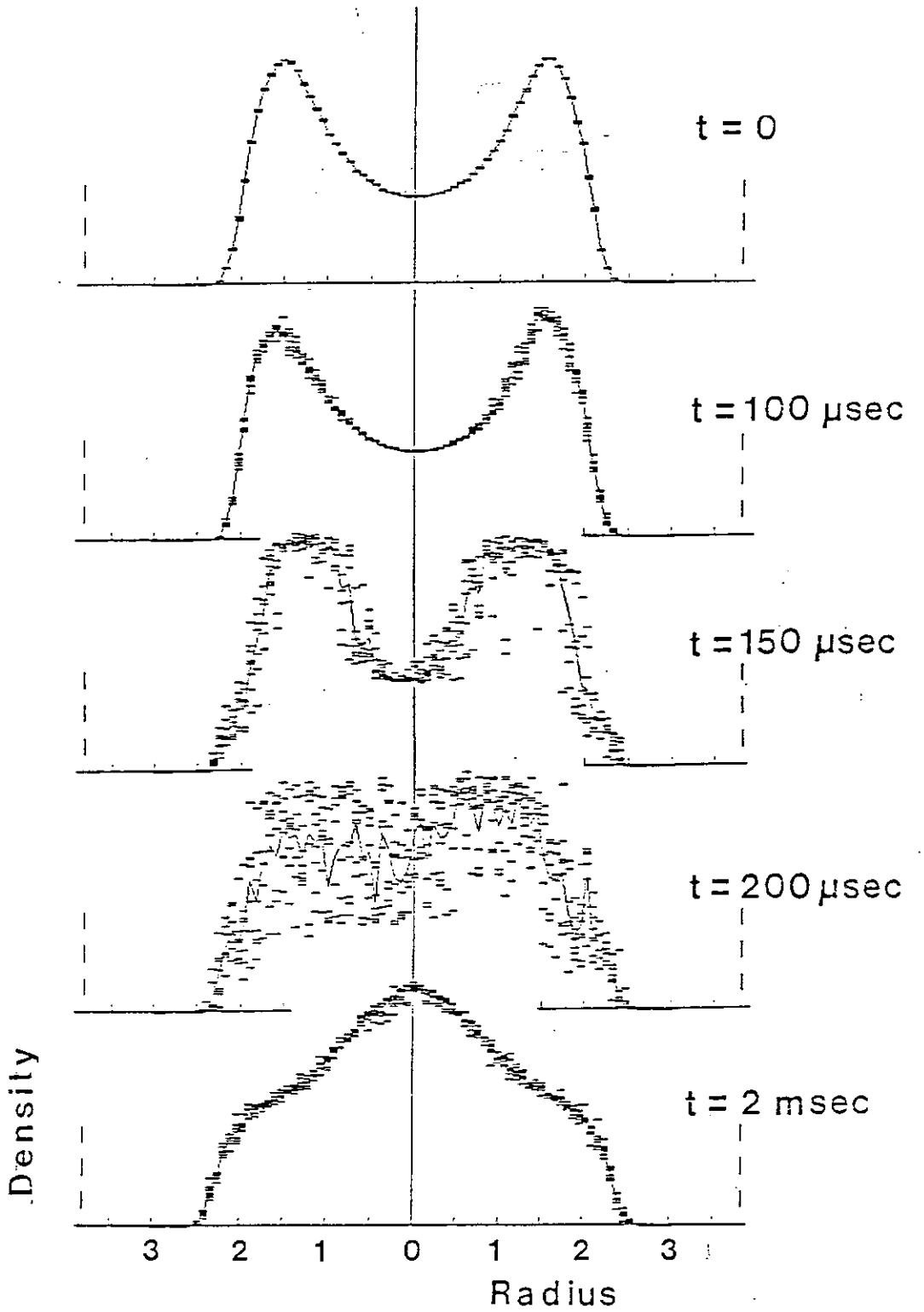

Figure 7. Plasma density vs. radius at various times.

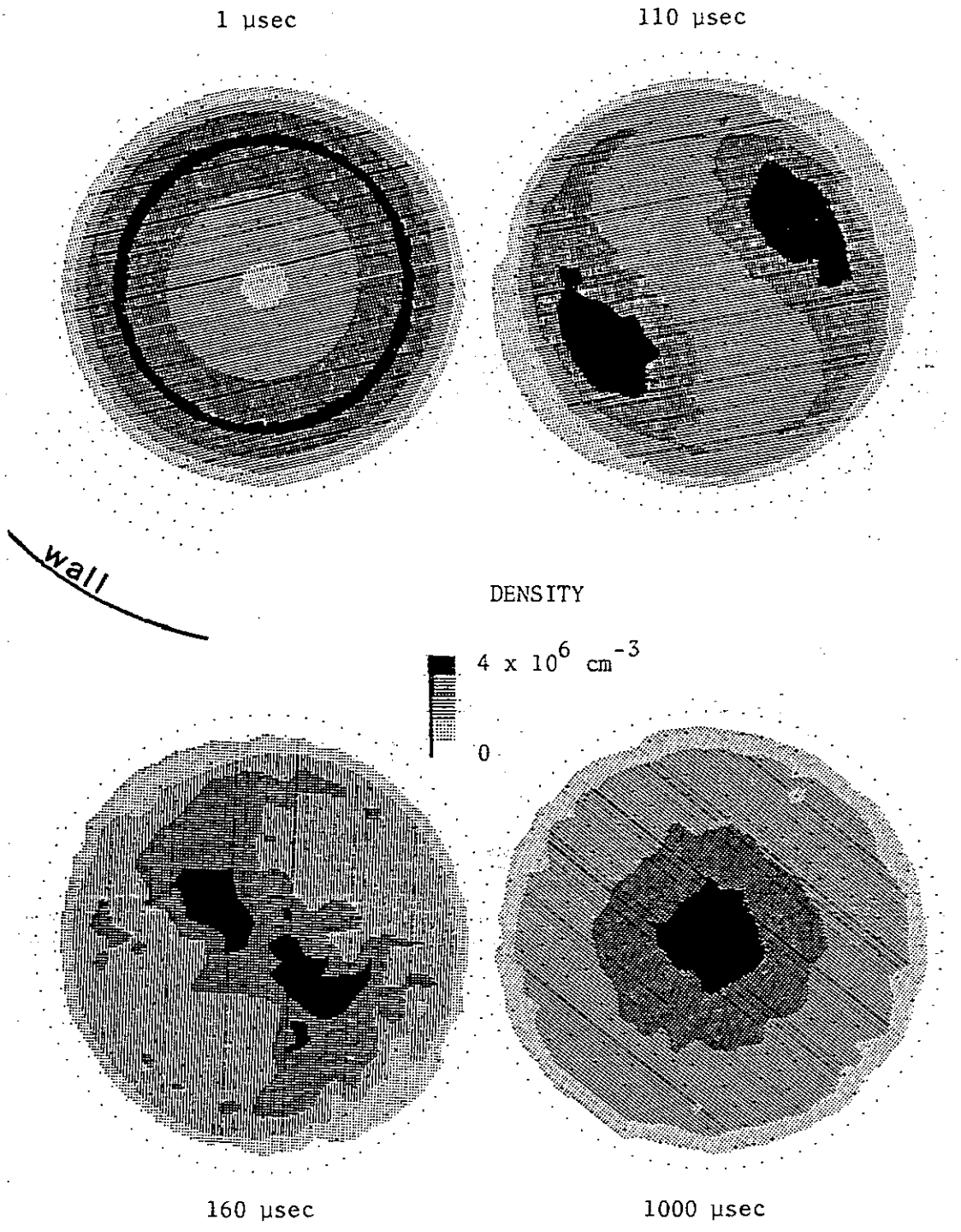

Figure 8. Two dimensional density plots showing $n(r,\theta)$ at 4 different times as an $\ell=2$ instability grows on a hollowed profile.

extended vortices.[32] From a theoretical point of view the 2-D $\mathbf{E}\times\mathbf{B}$ drift dynamics of these plasmas is mathematically isomorphic to 2-D incompressible inviscid flow of an ordinary fluid, so these plasmas may prove useful as model systems for studies of such fluids.

IV. EXTERNALLY-INDUCED TRANSPORT

The most important concept for discussing radial transport of a nonneutral plasma is the total canonical angular momentum of the charged particles.[6] The confinement is easiest to understand for the case where B is sufficiently large that we may set $P_\theta \approx (qB/2c)\sum_j r_j^2$. In the absence of external torques, the plasma cannot increase its mean square radius. We call rearrangements which conserve the mean square radius "internal transport" and transport which results from external torques "externally-induced transport."

There are a number of physical effects which can apply a torque on the particles and cause radial transport. In the regime of high neutral pressure, the dominant torque is due to electron collisions with neutral atoms.[4,33,34] For lower neutral pressure, the dominant torque is very likely due to asymmetric field errors.[34,35] The angular momentum removed by cyclotron radiation is typically negligible.[36]

Neutral Collisions

The effect of neutral collisions is studied by varying the neutral gas pressure. In Figure 9, the ordinate is the time, τ_m, required for the central density of an injected plasma to decay by a factor of 2. The abscissa is the pressure of helium which is bled into the machine. At helium pressures above 10^{-6} torr the plasma decay time varies inversely with neutral density.

Neutral transport due to electron-neutral collisions at a rate ν is given by

$$\frac{\partial n}{\partial t} + \frac{1}{r}\frac{\partial}{\partial r} r \left\{ -\frac{\partial}{\partial r}\nu r_L^2 n - \nu r_L^2 \frac{eE}{T} n \right\} = 0 . \qquad (1)$$

The first term in the bracket represents diffusion, which is roughly proportional to $\partial n/\partial r$; and the second term represents mobility, which is proportional to $E(r)$. It is worth noting that if the radius of the plasma is large compared to the Debye length then mobility, not diffusion, is the dominant transport process.[4] This equation is adequate as long as the electron distribution is adequately described by a rotating Maxwellian at temperature T. Of course, there is also a coupled equation describing $\partial(\frac{3}{2}nT)/\partial t$. This energy equation is generally dominated by the Joule

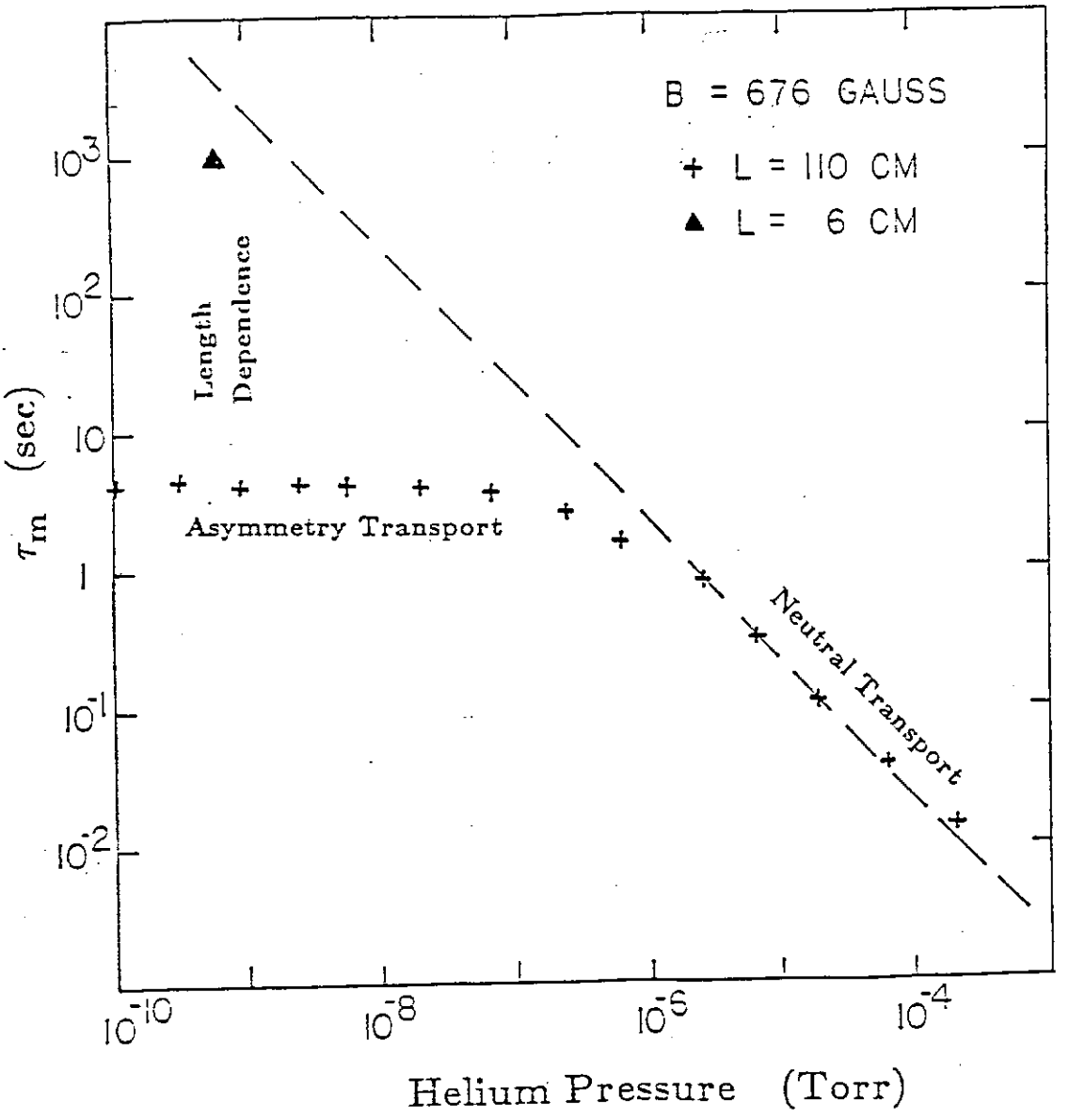

Figure 9. Plasma containment time τ_m versus helium pressure, showing neutral transport and asymmetry transport regimes.

heating (or cooling) which occurs when an electron moves outward (or inward) in the radial electric field. A detailed theory describing the evolution of the electron distribution function $f(r,v,t)$ has also been given for circumstances where electron-electron collisions are too slow to maintain a Maxwellian distribution.[33]

Detailed comparisons between theory and experiment have been made for transport in various regimes. Similarity solutions are obtained for the radial profile $n(r,t,P)$ for various pressures which depend only on r and Pt.[4] Analogous similarity solutions are observed for moderate variations in the magnetic field: the observed profiles depend on r and $B^{-2}t$. Theoretically obtained radial density profiles have been compared to experimentally measured profiles, using the profile at $t=0$ as the initial condition. Profiles predicted by the model are in good agreement with experiment.[4] It should be pointed out that in this case the density is fit as a function of both time and radius, not just one or the other. This provides a much more detailed test of theory than experiments which measure only a decay time constant or only a spatial decay curve.

Neutral collisions are not a dominant loss mechanism for any of the current apparatuses which operate at pressures of 10^{-10} Torr or lower. It is apparent from Figure 9 that at pressures below 10^{-7} Torr the radial transport is essentially independent of pressure.[34] We believe that the cause of the anomalous transport at low neutral pressures is small azimuthal magnetostatic or electrostatic asymmetries which couple angular momentum into the plasma.

Length-Dependent Transport

The anomalous loss is decreased when the plasma is made axially shorter.[35] The cylindrical wall of the apparatus is actually divided into sections of various lengths, and the plasma can be contained in any of these sections, enabling measurements of containment time, τ_m, vs length, L. The anomalous transport scaling is shown in Figure 10, where we plot τ_m vs L/B for all plasma lengths and magnetic fields studied on two separate apparatuses.[37] The data for each apparatus scales as $(L/B)^{-2}$ over more than five decades. Both data sets in Figure 10 show approximately a decade of variation around the general scaling lines. These variations are not a result of noise in the system, but rather represent reproducible effects. Different containment regions of equal length would be expected to have different error fields and generally give somewhat different containment times.

The newer apparatus, EV, represented by the solid points in Figure 10, was designed and built specifically to minimize field errors, with improvements in magnetic and electrostatic uniformity on both the long and short spatial scales. The fact that the containment times were enhanced by 20x in all parameter regimes suggests the dominance of a single loss

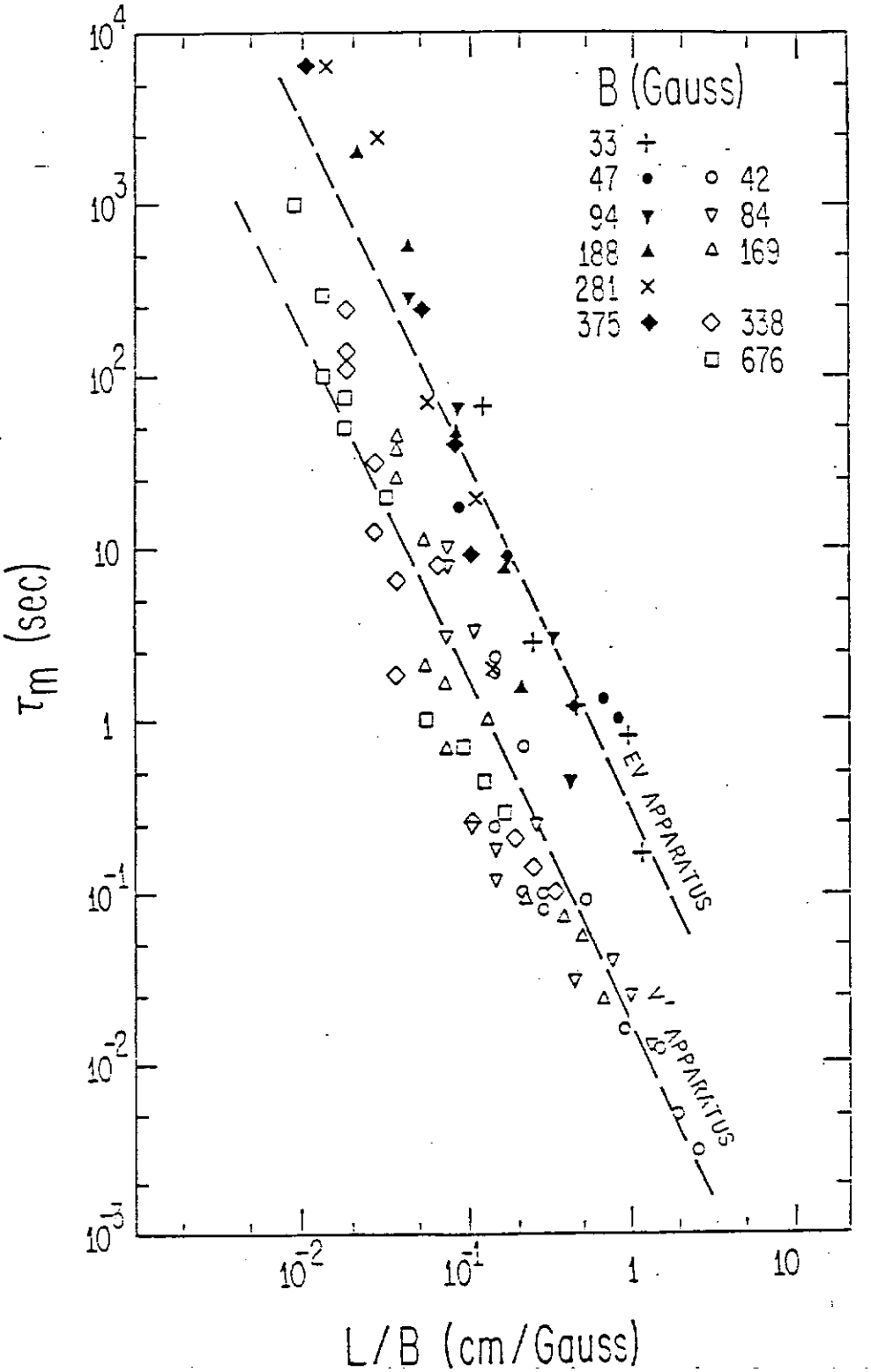

Figure 10. Plasma containment time τ_m versus plasma length L divided by magnetic field B, for two separate apparatuses.

mechanism, but the details of this process are not yet understood. Since all containment devices have asymmetries, we believe this transport will be generic to all non-neutral plasma experiments in this geometry. Of course, devices operating in different density or temperature regimes may have substantially different loss rates, and it is not clear that the lifetime of plasmas in the very short "Penning trap" geometry[38] will fall on the curve.

Applied Asymmetries

To unravel the underlying physics associated with the anomalous transport, we deliberately apply asymmetric fields to the plasma. Since the residual transport is very small, the transport due to deliberately applied nonaxisymmetric fields can be made to dominate. This method allows us to modify at will the amplitude, wavelength, and time dependence of the perturbations and observe the resulting transport.

Most of our experiments studied transport due to applied electric field asymmetries.[39,40] The basic experimental sequence is as follows: After a plasma sample is captured, a non-axisymmetric perturbation is applied by putting a signal of frequency ω on one or more azimuthal sectors, sometimes with different phase on different sectors. After a variable time, the perturbation is turned off and then the electrons are dumped longitudinally. Electrons are collected by a radially moveable probe and the line-integrated density is obtained. Since the shot-to-shot variation of the plasma density is less than one percent, radial density profiles can be constructed by changing the probe position between shots [Fig. 11]. If the perturbation is applied only on alternate shots, the collected signal may be analyzed with a lock-in amplifier and the density change $\delta n(r)$ due to the perturbation is obtained [Fig. 11]. The effect on $\delta n(r)$ as parameters of the plasma and the perturbation are varied can be studied.

It is useful to conceptually divide this transport problem into two parts. First it is necessary to determine the collective response of the plasma to an externally applied asymmetry, that is, to determine the asymmetric fields which exist in the plasma. Then, it is necessary to determine the transport produced by these fields. This second part of the problem is determined by a transport equation. Of course, the solution to the first part of the problem must be inserted into the transport equation. The fields in the plasma can be very different in magnitude than the applied field. For example, under certain conditions an applied electric field is shielded out of the plasma, and under other conditions it is greatly enhanced in the plasma. The enhancement occurs when the applied field contains wave number and frequency components which correspond to a normal mode of the plasma. An enhanced asymmetric field in the plasma generally produces an enhanced level of transport. Figure 12 shows the perturbation induced density change at $r=0$ as a function of applied frequency. The peaks in this curve correspond to various plasma resonances. The data demonstrate that the

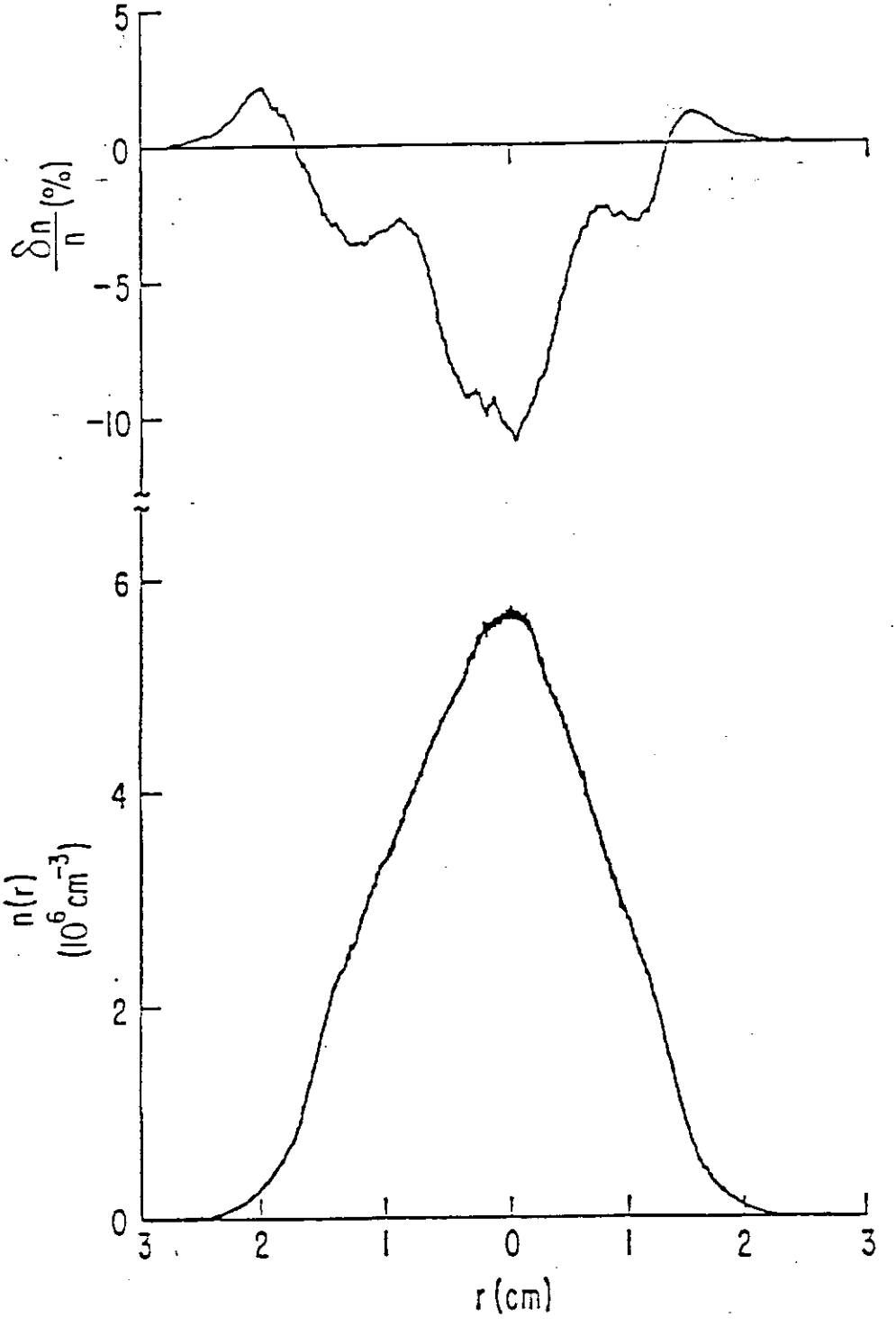

Figure 11. Plasma density profile n(r); and density change δn(r) induced by a non-axisymmetric perturbation.

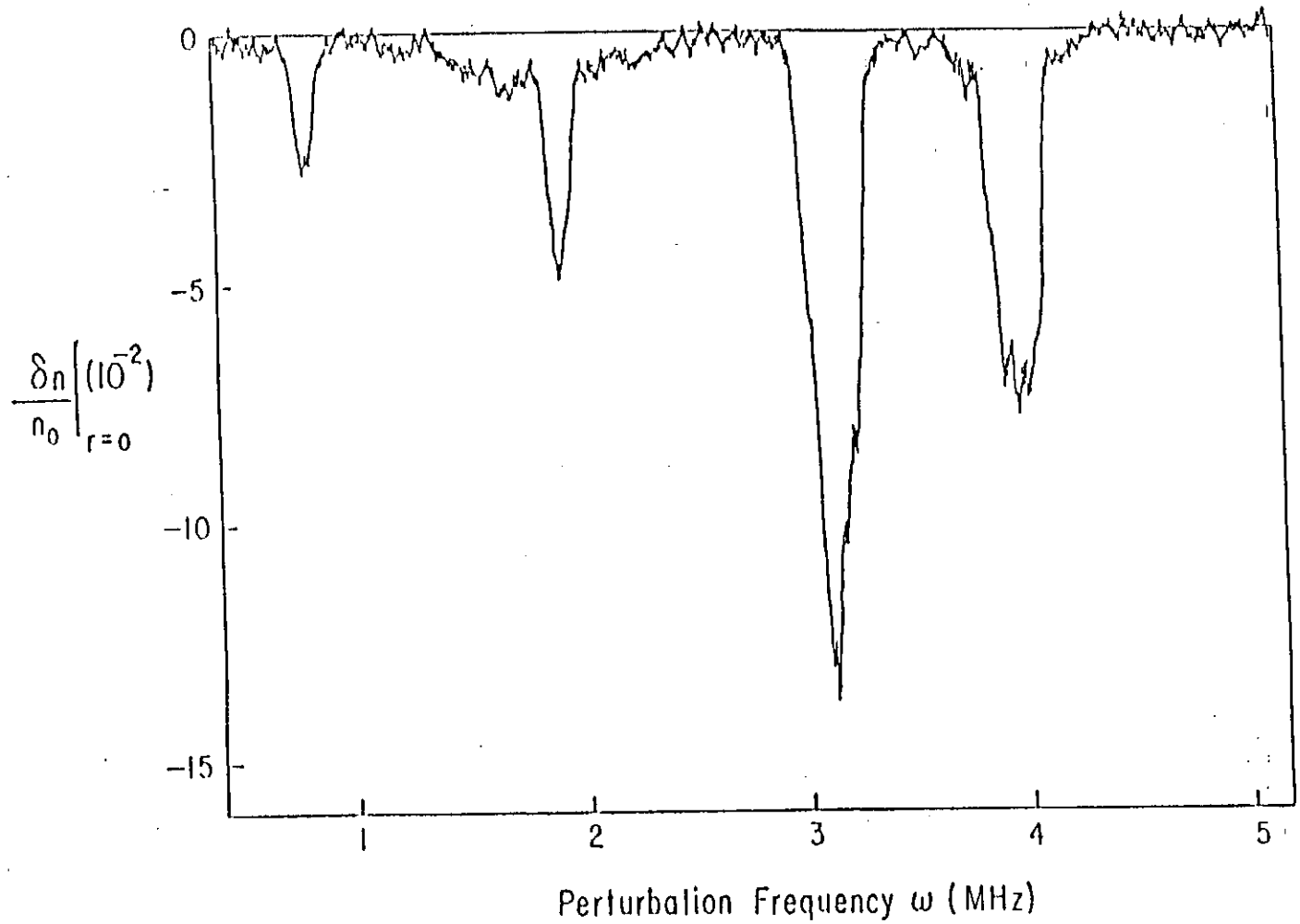

Figure 12. Induced density change δn(r=0) versus the frequency ω of the applied perturbation.

radial transport is enhanced up to twenty-five fold when the applied perturbation frequency is near a normal mode frequency of the plasma column.[39]

The enhancement may occur even for static asymmetries ($\omega = 0$), since the plasma rotates. A normal mode which propagates backward (upstream) on the column can have zero frequency in the laboratory frame and be driven resonantly by an applied field asymmetry. In the demonstration of Figure 12, for experimental convenience the frequency was tuned to demonstrate the resonance effect, but in general to avoid enhanced transport it is necessary that the plasma not be inadvertently tuned so that a resonance occurs for $\omega = 0$.

For some experimental studies there is an important advantage to launching at a mode frequency. In general, the probes launch many modes with various values of k and l. When the signal is applied at a mode frequency, a single mode with known spatial properties dominates the transport and the situation is greatly simplified.

The scaling of radial transport with the amplitude of an electrostatic asymmetry has been studied. The amplitude of the field in the plasma is determined by applying the perturbation at a normal mode frequency and monitoring the amplitude of the mode with a second wall probe. In some, but not all cases after an initial transient, the mode amplitude is linearly proportional to the applied perturbation and the radial transport scales as the square of this amplitude. These observations are consistent with the predictions of resonant particle transport theory in the "plateau regime:"[41] the scaling is expected to be different in other regimes. However, these measurements are not sufficient to conclude that detailed verification of this part of the theory has been obtained.

Another instructive variation in the way the perturbation is applied to the plasma is possible. Since there are sector probes at various angles in the apparatus, the perturbing signal may be applied with a different phase at different angles to produce an electrostatic perturbation with angular phase velocity either faster or slower than the column rotation.[39] Data are shown in Figure 13. The ordinate is the change in density at $r = 0$ produced by the perturbation. The abscissa is the azimuthal phase velocity of the perturbation. The peaks in this curve correspond to various plasma wave resonances. The angular rotation velocity of the center of the plasma is indicated by the arrow. It is important to note that perturbations with a phase velocity slower than the central plasma rotation velocity produce plasma loss at the center, whereas perturbations with rotation velocity larger than the plasma rotation velocity produce an increase in density at the center. In this latter case we are adding angular momentum to the plasma and pumping the particles inward. It may be possible to use this effect for desirable manipulations of the plasma. It should be noted that the analogous procedure using lasers to provide the radiation pressure in the θ direction is already well developed.[38]

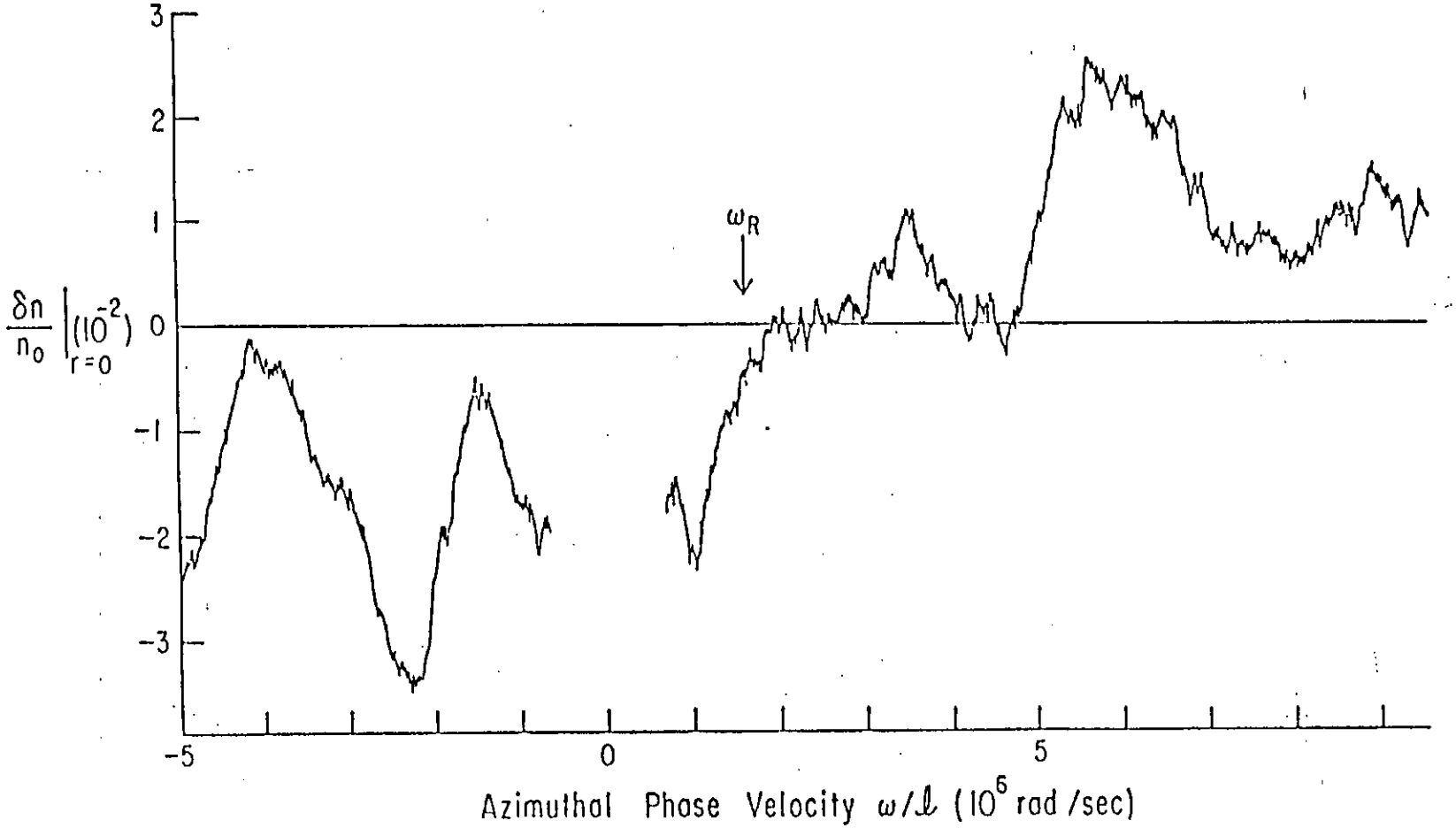

Figure 13. Perturbation induced density variation at r=0 vs. azimuthal phase velocity of perturbation.

We have also studied transport produced by applied magnetic asymmetries. The results are similar to those for the electrostatic case. If electric and magnetic asymmetries are applied at the same time in such a way that the $\mathbf{E}\times\mathbf{B}$ drifts due to the electric perturbation opposes the grad-B drifts due to the magnetic perturbation, then the net transport is less than that produced by either the electric or magnetic asymmetries alone. This latter result is in harmony with the basic theoretical framework that the transport is produced by guiding center drifts. It also supports the idea that the experiments with electrostatic asymmetries are not fundamentally different from those with magnetic asymmetries.

Induced Instabilities

The experimental results above demonstrate how linear collective effects can enhance radial transport. Field asymmetries can also affect the *stability* of a nonneutral plasma.[40,42,43] For a rotating plasma, a static field asymmetry can act as a pump for various wave instabilities. Two examples are the decay instability and the induced-scattering instability. For the decay instability, the field asymmetry excites two unstable daughter modes. These modes (one positive energy and one negative energy) must have frequencies that satisfy a resonance condition $\omega_1+\omega_2\approx 0$. For the induced-scattering instability, one of these modes is in effect replaced by resonant particles. These particles have axial velocities close to the phase velocity of the beat wave formed by the remaining mode and the pump. For this process, only one unstable mode is produced and, since generally a broad range of particle velocities is present, no sharp frequency resonance condition is required. Both types of instability allow field asymmetries to transfer angular momentum to the plasma and thus are associated with enhanced radial expansion.

Several features of the instability which has been observed identify it as due to induced scattering: (1) Only one growing mode is observed. The mode is a standing electron plasma wave with azimuthal and axial wave numbers $l_m=0$, $k_m=\pi/L$. The wave becomes unstable when a threshold condition is exceeded and eventually saturates after growing 40-50 dB. (2) The threshold and growth rate of the instability depend on the amplitude of static field asymmetries. (3) The presence of the instability is associated with an enhanced level of radial transport. This is significant since an azimuthally symmetric wave ($l_m=0$) does not by itself produce a radial drift of particles. (4) The instability occurs over a broad range of plama parameters.

According to theory[43], the time evolution of the observed mode is governed by the equation

$$dA_m/dt=\left[-|\gamma_m|+\Gamma|A_w|^2\right]A_m\ , \qquad (2)$$

where γ_m is the mode damping rate in the absence of field asymmetries, A_m is the mode amplitude, A_w is the field-asymmetry amplitude at the wall of the device, and Γ is the total beat-resonant coupling coefficient. When the bracketed term is positive, the mode is unstable and grows exponentially. Assume for now that $\Gamma > 0$. Since any real plasma device will have small asymmetries due to construction imperfections, A_w is always nonzero. In the experiments these small asymmetries are sometimes large enough to exceed the threshold condition and then the instability appears as soon as the plasma is captured. Such a case is shown by curve *a* in Fig. 14. The wave starts to grow immediately after the injection gate is closed ($t = 0$). The mode growth may be prevented in accordance with Eq. (2), by increasing the value of $|\gamma_m|$. One way to do this is by placing a resistive load between a 360° ring probe surrounding the containment volume and ground. Wall currents induced by the positive energy symmetric plasma wave flow through this load and dissipate wave energy. This creates additional mode damping beyond that produced by wave-particle effects. (Angularly dependent diocotron modes do not couple to a 360° probe and are unaffected.) The stabilizing effect of such an addition is shown by curves *b* and *c* in Fig. 14. Curve *b* shows that the plasma remains stable until the resistive load is removed at the time indicated by the lower arrow, after which time the wave begins to grow. For curve *c*, the instability is quenched by the addition of the resistive load at the time indicated by the upper arrow.

The theoretical equation also predicts that a stable plasma will be destabilized by an increase in the magnitude of the field asymmetry. To demonstrate this effect the injection conditions are adjusted to create a stable plasma. Shortly after injection ($t = 5$ ms) a static field asymmetry is applied to the plasma by placing equal and opposite voltages on opposing 180° sectors. The $l_m = 0$ mode is then driven by applying a short (75 μs) tone burst at the mode frequency to a ring probe. When no asymmetry is applied, the mode damps away after the tone burst ends. As the asymmetry amplitude is increased, the mode becomes more lightly damped and finally becomes unstable. The change in growth rate varies as the square of the asymmetry amplitude as expected from Eq. (2).

According to theory[43], a destablizing (i.e. positive) contribution to Γ requires $l_a \omega_R > \omega_m$, where ω_m is the mode frequency, ω_R is the rotation frequency of the center of the plasma column and l_a is the angular mode number of the applied asymmetry. A simple physical explanation for this condition is possible. In the frame of the rotating column, $l_a \omega_R$ is the frequency of the field asymmetry (which is static in the lab frame). The mode frequency, ω_m, is the same in both frames since $l_m = 0$. The inequality then expresses the requirement that the pump frequency must exceed the mode frequency in order for energy to flow from the pump to the mode. If a given l_a does not satisfy the inequality, it will make a negative contribution to Γ and thus tend to increase the mode damping.

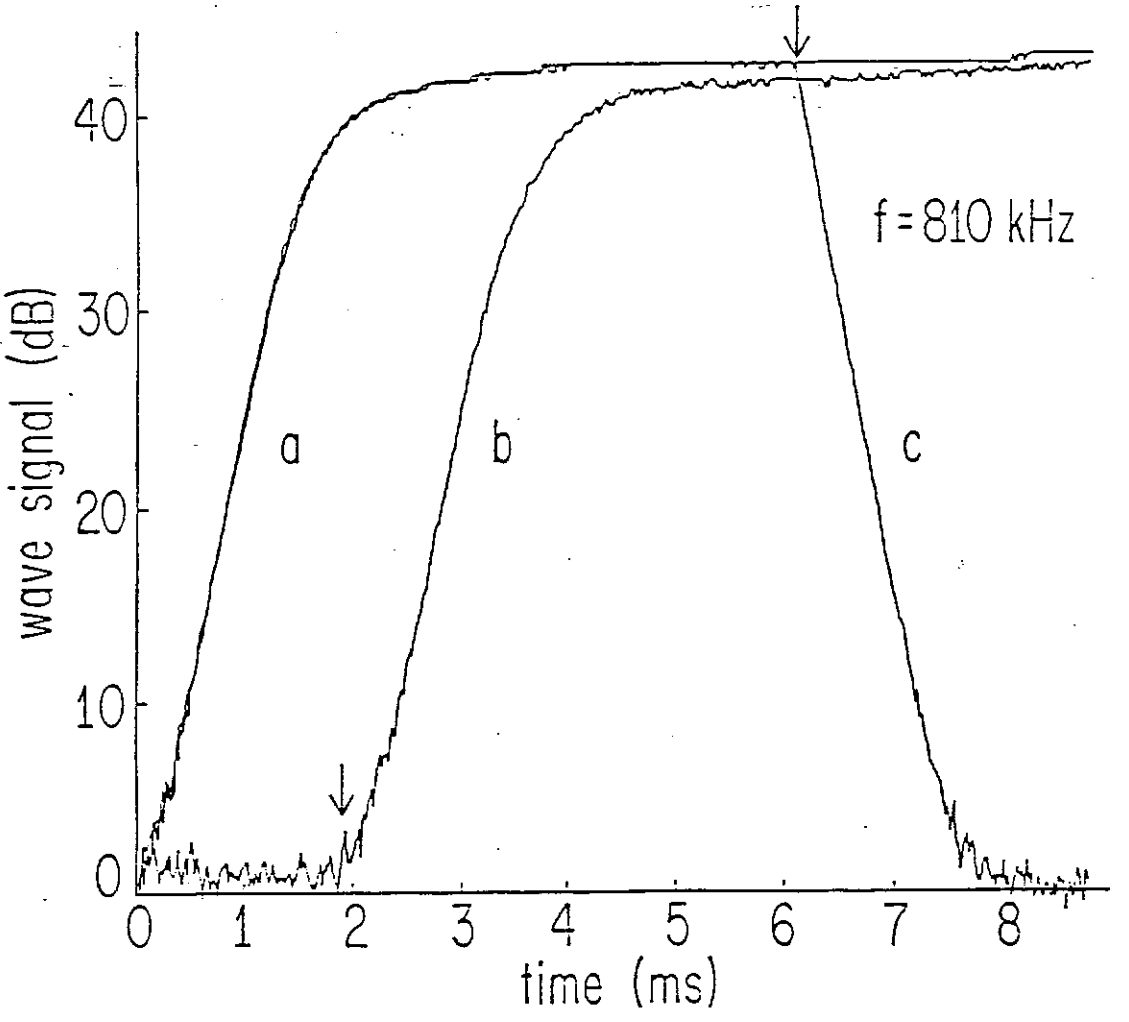

Figure 14. Unstable $\ell = 0$ wave amplitude vs. time.

For our experimental parameters, the above inequality reduces to $l_a \geq 3$. When the external perturbation is launched off resonance, high angular components from the sector probe dominate and the $l=0$ mode is driven unstable. If the perturbation frequency is selected so as to drive the $l=1$, $k=0$ diocotron mode resonantly, the $l_a=1$ component of the asymmetry in the plasma dominates and damping of the $l_m=0$ mode increases as expected from theory.

V. INTERNAL TRANSPORT

In a sufficiently symmetric apparatus, particle-particle interactions will cause the plasma to evolve close to a confined thermal equilibrium before external torques cause appreciable expansion of the plasma. Our newest machine, EV, was designed to minimize losses due to field errors. The resulting long containment time for the shortest plasmas has enabled observation of transport to global thermal equilibrium.[44] The plasma evolves to a state in which the temperature is radially uniform and the density profile is such as to give rigid drift rotation, as expected. However, the time required for transport to equilibrium differs significantly from the predictions of traditional like-particle transport theory:[45–47] the equilibration times are orders of magnitude smaller, and scale approximately as B^1 or B^2 instead of as B^4.

Experimentally, we measure the number of electrons remaining on field lines at a given radius,

$$Q(r,t)=A\int_{-\infty}^{\infty} dz\, n(r,z,t) \quad , \tag{3}$$

where A is determined by the collimator hole area and by absolute calibrations of the amplifier gains and capacitances. Here, we assume that the plasma has rotational symmetry and ignore the azimuthal variable θ. We measure $T_\perp(r,t)$ with the analyzer previously discussed. Velocity-space isotropization occurs in a few collision times (milliseconds), giving $T_\perp(r)=T_\parallel(r)\equiv T(r)$.

Since the plasma is short and its ends are not perfectly flat, the plasma length is a significant function of radius. The density $n(r,z)$ is obtained from the measured z-integral $Q(r)$ by numerically solving a 2-D Poisson equation. Using the known boundary conditions on the cylindrical wall allows us to solve for the self-consistent solution for $n(r,z)$ and $\phi(r,z)$. From n, ϕ, and T, we can immediately calculate the drift velocity $V_\theta(r)$, so we obtain all the information needed to test the "fluid" description of the plasma.

An example[44] of the experimentally measured evolution towards global thermal equilibrium is shown in Figure 15. The density profiles $n(r,z=0)$ and rotation profiles $\omega(r)=V_\theta(r,z=0)/r$ at three different times are given.

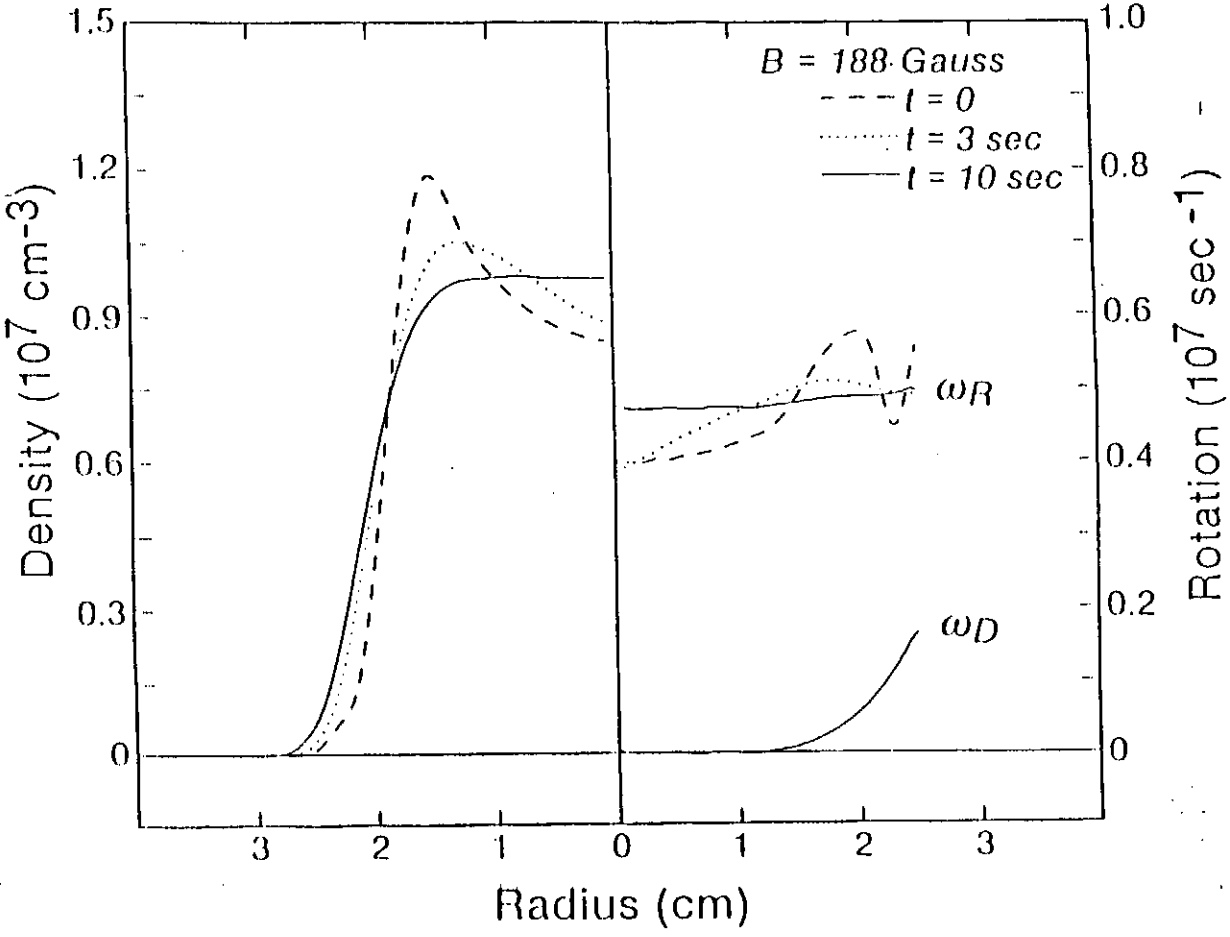

Figure 15. Experimental plasma density profiles n(r,t) and rotation profiles $\omega_R(r,t)$ at three different times t, showing the evolution to equilibrium. Also shown is the diamagnetic drift $\omega_D(t)$ at t = 10 sec.

Also shown is the diamagnetic drift $\omega_D(r)$ at $t=10$ sec. Initially, the density is low in the center and peaked at the edge. This *short* plasma is observed to be stable even though its radial density profile is nonmonotonic. This profile evolves towards a shape which appears to be a thermal equilibrium profile:[45] it is essentially constant out to some radius and then falls to zero on the scale of the Debye length. Of course, the true test of the density profile being that of equilibrium is whether the rotation profile is uniform. As shown in Figure 15, the initially injected plasma has substantial shear, rotating about 40% faster on the edge than in the center. As particles and heat are transported radially, the rotation profile evolves to essentially rigid rotation. Although not shown here, the temperature profile also becomes uniform during this evolution.

To obtain a characteristic time, τ_{eq}, for the particle transport towards equilibrium, we calculate how "far" the density profile at any given time is from the final equilibrium profile. This "distance" $D(t)$ is essentially the radial integral of the difference between the rotation profile at a given time and the final rotation profile. As shown in Figure 16, $D(t)$ decreases as $e^{-t/\tau_{eq}}$ as the plasma relaxes toward equilibrium, and τ_{eq} is unambiguously determined.

Using this method[44], we have obtained characteristic times τ_{eq} over a range of fields B from 47 to 470 G, as shown by the solid triangles in Fig. 17. We find that τ_{eq} scales closely as B^1, implying transport rates scaling as B^{-1}. For this series, we tried to keep the initial plasmas as alike as possible as B was varied. For all but the lowest magnetic fields, the initial $Q(r)$ was uniform out to the plasma edge, after which it dropped sharply; for the lowest fields, $Q(r)$ was more nearly Gaussian. This monotone decreasing $Q(r)$ corresponds to a non-monotonic $n(r)$ and $\omega(r)$. Initial plasma temperatures were typically uniform at about 0.8 eV.

We have previously estimated the equilibration times for substantially different plasma profiles at slightly higher densities, using much less rigorous techniques. These rough estimates for τ_{eq} scaled approximately as B^2. The two data sets differ most at low magnetic fields where these rough estimates are generally least reliable. These two data sets were obtained from substantially different initial plasmas, and it is now predicted theoretically that the dominant transport mechanism depends on the plasma density profile.[48,49]

The experimental scaling of $\tau_{eq} \propto B^1$ for plasmas with non-monotonic $\omega_E(r)$ stimulated theory development for this case. This theory[48] predicts that a new non-local "resonant rotation" transport mechanism will be important when $\omega_E(r_1)=\omega_E(r_2)$ for some r_1 and r_2 in the plasma, and that transport times from this process alone should scale as B^1. The transport rates are difficult to compute for realistic plasmas, but estimates are consistent with the experimental data. In contrast, when $\omega_E(r)$ is monotonic, theory predicts that only the local "collisional $\mathbf{E}\times\mathbf{B}$ drift" transport[49] should appear. Transport times would then scale approximately

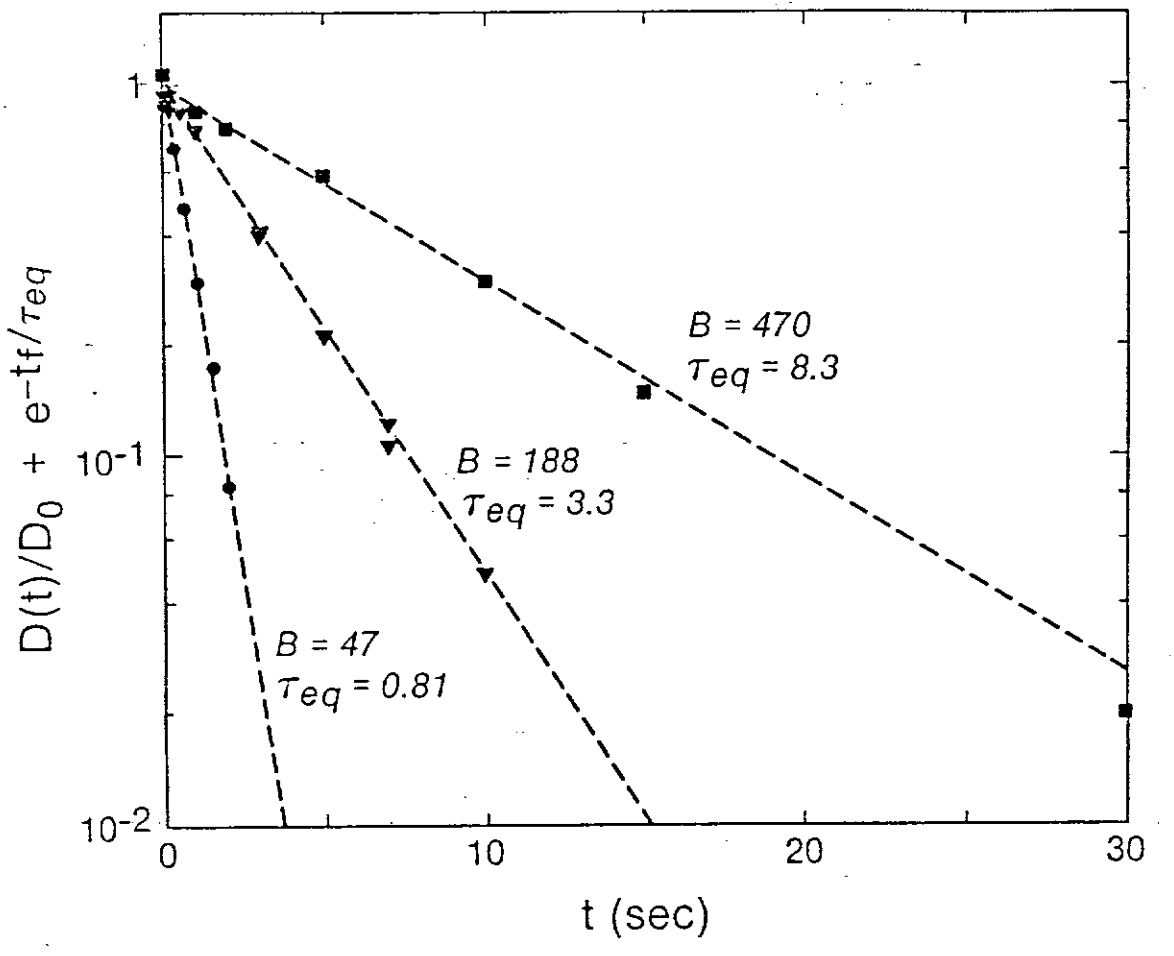

Figure 16. Measured "distance" from equilibrium D(t) vs. time for B = 47, 188, and 470 G. The dashed lines show exponential fits to obtain τ_{eq}.

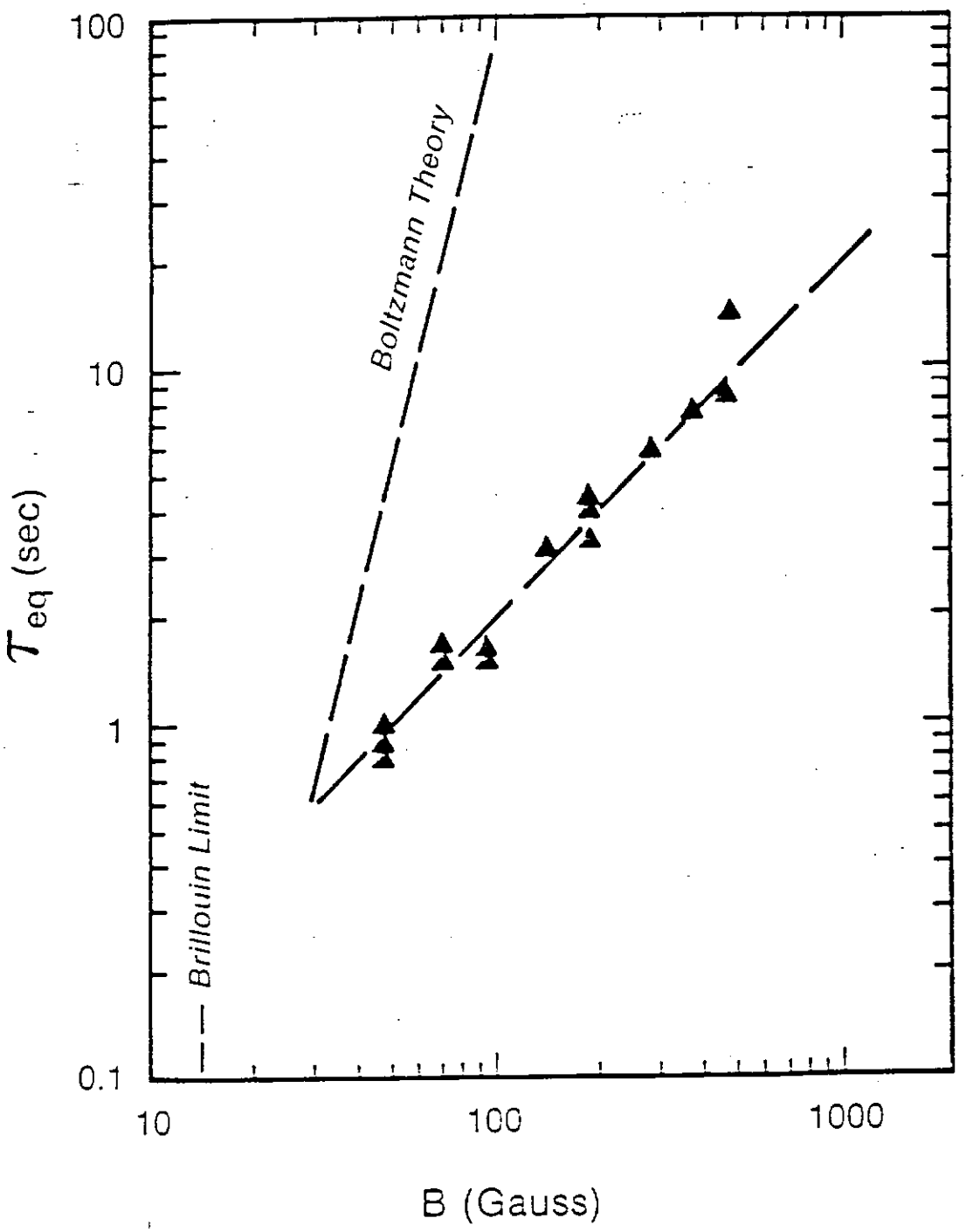

Figure 17. Experimental density equilibration times τ_{eq} vs magnetic field B. The dashed line through the data represents $\tau_{eq} \propto B^1$; the upper dashed line is the prediction of traditional Boltzmann theory, scaling as B^4.

as B^2.

These experiments clearly show that a new type of transport much stronger than that predicted by traditional like-particle transport theory is operating in these plasmas; but the experiments do not yet verify any particular theory. The possibility of two new transport processes makes the experiments more interesting, but makes the experimental analysis more difficult. Detailed data which might provide a clear demonstration of these two scalings are not yet available.

VI. ANISOTROPIC TEMPERATURE RELAXATION

The relaxation rate due to collisions of an anisotropic temperature distribution has been measured.[8] In these experiments, the parallel temperature $T_\parallel$ is changed by axial compression or expansion, and then the time evolution of $T_\parallel$ and $T_\perp$ is measured as they relax to a common value. This yields a relaxation rate which can be obtained as a function of density and temperature. For the purposes of this experiment, long confinement times (much longer than any other time scale of interest) are important, in that they allow the thermal evolution experiments to be conducted at constant energy and density.

The experimental procedure is as follows. The plasma is captured and allowed to come to thermal equilibrium. Then time varying potentials are applied to appropriate cylinders to axially compress or expand the plasma on a time scale much longer than the axial bounce time yet much shorter than the relaxation time. The compression or expansion thus preserves the adiabatic bounce invariant $J = \int v_\parallel \, dz$. The result is essentially a one-dimensional compression or expansion with $T_\parallel$ changed by the ratio $(L_2/(L_1+L_2))^2$, and $T_\perp$ unchanged, creating an anisotropic temperature distribution. After allowing the initial anisotropy to evolve for a time t, we dump the plasma axially and measure $T_\parallel$, $T_\perp$, and the plasma density. We construct the time evolution of the anisotropy from a number of machine cycles of varying evolution time t. This procedure relies on shot-to-shot reproducibility, which is generally better than 1%. All of our rates are obtained from temperatures measured on the axis.

Figure 18 shows the time evolution of $T_\perp$ and $T_\parallel$. Initially the plasma is captured and evolves to an isotropic temperature $T = 1.47$ eV, and to a density profile which is essentially constant over the area of the collimator hole. At $t = 0$, the plasma is expanded axially. The perpendicular temperature is unchanged but the parallel temperature drops to 0.5 eV. Then $T_\perp(t)$ and $T_\parallel(t)$ are measured as they relax towards the common equlibrium value of $T_{eq} = 1.08$ eV. The $T_\perp$ curve is a better measure of the decay rate than the $T_\parallel$ curve since the parallel temperature is measured on the high velocity tail of the distribution function which relaxes at a slower rate than do the thermal particles. The $T_\perp$ decay curve is fit with the almost exponential prediction of theory[50] to give the relaxation rate.

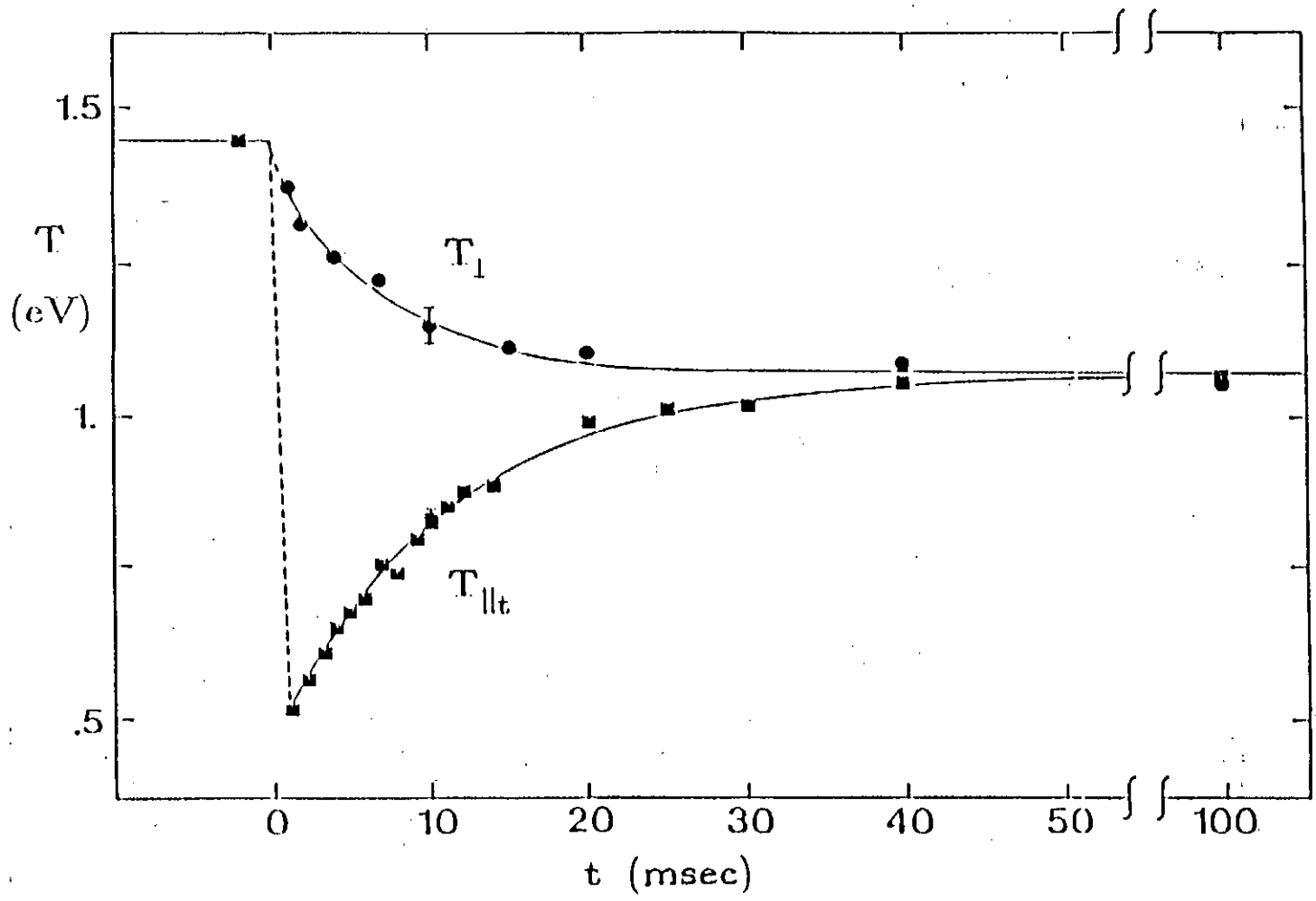

Figure 18. Temperature evolution as a function of time.

A theoretical description of collisional velocity scattering has been the subject of continuing effort over the past 50 years. Small momentum transfer collisions are thought to dominate, which has led to a Fokker-Planck approximation to the velocity scattering process. Ichimaru and Rosenbluth[50] (IR) calculate the rate of anisotropic temperature relaxation in a weakly magnetized one-component plasma for which the Larmor radius r_L is much larger than the Debye shielding length λ_D, i.e. $r_L >> \lambda_D$. They employ the "dominant term" approximation, which neglects all terms that do not contain the Coulomb logarithm, $\ln\Lambda$, factor in the rate. Since terms of relative order $1/\ln\Lambda$ are neglected, the theoretical rate is calculated only to that accuracy, which in our plasma is about 10%.

We can adapt the small magnetic field calculation of IR to our experimental regime of $r_L << \lambda_D$ by using a general result of Montgomery, Joyce and Turner[51] (MJT). MJT have shown that, to good approximation, zero and small magnetic field transport theories can be applied in the $r_L < \lambda_D$ regime if the argument of the Coulomb logarithm is changed from $\Lambda = \lambda_D / b$ to $\Lambda = r_L / b$, where $b = e^2/T$ is the classical distance of closest approach. This change can be thought of as a decrease in the range over which effective collisions can occur. The effect of the MJT approximation in our experimental regime is to reduce the theoretical rate of IR by approximately 25%.

The experimental results[8] agree with the predictions of this theory to within approximately 10% over a two decade range, as shown in Fig. 19. This is an absolute comparison, since there are no adjustable parameters in either the theory or the experimental measurements. In this data, the density is varied between 3×10^6 and 3×10^7 cm^{-3}, and the temperature is varied between 0.7 and 8 eV, while the magnetic field is held constant at 280 Gauss. The line is the absolute prediction of the collisional relaxation theory.

We do not believe that collective instabilities have significantly contributed to the measured rates, since the agreement with theory is so good. An instability driven by the temperature anisotropy could contribute to isotropization. However, linear stability theory predicts suppression of the Weibel or Weibel-like instability in our parameter regime. Furthermore, the agreement of measured rates from both the $T_\perp/T_\parallel < 1$ and $T_\perp/T_\parallel > 1$ anisotropy data argues against significant isotropization due to instability, since typically only one type of anisotropy may lead to growth.

For the experiment just described, $b << r_L << \lambda_D$ where b, r_L and λ_D are the classical distance of closest approach, the larmor radius, and the Debye length, respectively. If the plasma is cooled so that $r_L \sim b$ the standard theory is inapplicable and when $r_L << b$ the effect of a new many particle adiabatic invariant of O'Neil and Hjorth[52,53] should result in a collision rate that decreases sharply as the temperature decreases. Putting in numbers for electrons gives $T^{3/2}[\mathrm{eV}] << 10^{-7}\,\mathrm{B}\,[\mathrm{gauss}]$ so even for large magnetic fields, low temperatures are required to see these effects. An

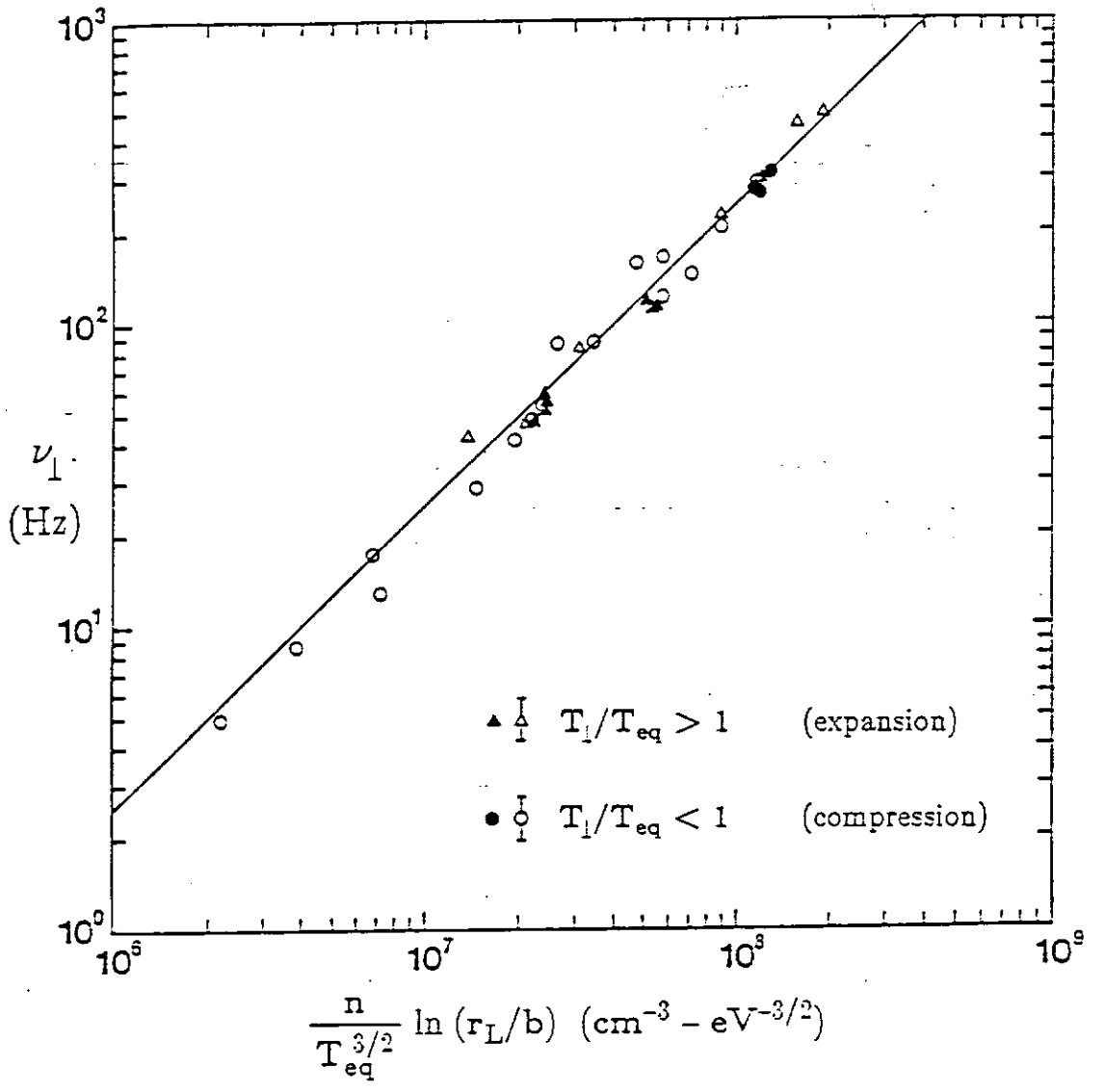

Figure 19. Experimentally measured relaxation rates for various electron plasma densities and temperatures. The solid line is the absolute prediction of theory. Solid symbols have statistical errors of ≈ 3%, open symbols ≈ 15%. B_z is 281 G.

experiment to measure the relaxation rate in this regime will be described in the next section.

The Cryogenic Plasma

It is interesting to inquire what will happen if the electron plasma is cooled to a very low temperature, by cyclotron radiation, for example. One thing that *cannot* happen is recombination, since there are negligibly few ions in the confinement region. Rather, as the temperature is reduced, a whole series of novel states of matter should be obtained, including liquids and solids, with various novel collisional and quantum-mechanical effects. Since we expect these states of matter at a few degrees Kelvin or less, we call them collectively the "cryogenic plasma."

We have built an apparatus [CV] designed to make cryogenic pure electron plasmas. The apparatus is based on an 18" long superconducting magnet with a 2.5 inch diameter bore, giving a field up to 80 kG. In this bore, at LHe temperature, is a sealed vacuum can containing the containment electrodes. The filament is positioned in the fringing field of the superconducting solenoid and the electrons are pushed electrostatically into the strongly converging magnetic field, in a manner similar to the "Brillouin flow" injection used for high current beam devices.[54] The radius of the captured plasma reflects the convergence of the field lines. This technique gives surprisingly quiescent plasma injection at considerably higher densities than can be obtained when the filament is in the strong field region. Furthermore, this technique eliminates the need to ramp the magnetic field on each shot from the low fields in which the filament can operate to the high fields required for plasma cooling.

The temperature evolution of the plasma is determined by the balance between heating and cooling rates.[7] The plasma heats when it expands, due to transfer of space charge electrostatic energy into electron kinetic energy. By measuring the temperature evolution under conditions of rapid radial expansion, we have been able to determine that most (75%-100%) of this energy does in fact go into heating. Normally, we operate with parameters giving long expansion times, up to 10^5 sec. The plasma cools because electrons emit cyclotron radiation which is then absorbed at the LHe-cooled walls. A single electron radiating into free space would lose energy according to the well-known Larmor formula, giving exponential cooling with an e-folding $\tau_c = (0.24 \text{ sec})(B/40 \text{ kG})^{-2}$. The measured rate of cooling is typically with a factor of 2 of the single electron rate.

Typically, we confine a plasma of density 1.8×10^{10} cm^{-3} in a field of 41 kG, with a characteristic expansion time of 2×10^5 sec. Under these conditions, the plasma should cool to approximately 6 °K, giving a correlation parameter $\Gamma \equiv (e^2/kT)(4\pi n/3)^{1/3} \approx 1$, indicating that the system should be near a locally ordered liquid.[7] This temperature is low enough that the cyclotron action is quantized into the Landau levels.

This plasma cooling has been verified down to 50°K by direct measurement. In Figure 20 the measured temperatures start at about 2×10^6 K and cool to 50 K (or less) in 3 seconds. The two kinds of symbols distinguish different circuits used for an electronic test which is unimportant to the present description of the experiment. We believe that the leveling off at about 50 K represents a limitation caused by instrument noise and does not give the true plasma temperature.

This cryogenic plasma has been used to extend the measurement of relaxation rate of an anisotropic temperature distribution into the strongly magnetized regime.[55] The experimental method is modified somewhat in this parameter range. In the cryogenic case an oscillating component is added to the containment voltage to modulate the length of the plasma, and plasma heating as a function of the modulation frequency is measured. If the modulation is slow compared to the relaxation rate, the compression is three-dimensional and reversible so there is no heating. If the modulation is slow compared to the bounce frequency but rapid compared to the relaxation rate, the compression is one-dimensional and reversible, and again there is no heating. The plasma heating is a resonant effect which occurs when the modulation frequency and relaxation rate are equal. We measure this resonance curve as a function of plasma temperature to obtain the relaxation rate as a function of temperature.

Preliminary results of this measurement[55] are shown in Figure 21 which gives the modulation frequency which produces maximum heating, f_{max}, as a function of plasma temperature. The line is sketched through the points to aid the eye: it is not theory. At low temperatures the relaxation rate, $\nu_\parallel$, increases with increasing temperature, peaks near the temperature where $r_c = b$ and then decreases with increasing temperature. This behavior of $\nu_\parallel$ at low temperature in the strongly magnetized regime is consistent with the theory of O'Neil and Hjorth which is based on the new many-particle adiabatic invariant.[52,53] For $r_c \gtrsim b$ our results test the dependence of $\nu_\parallel$ on the Coulomb logarithm, $\ln r_c/b$ and determine where that approximation fails. In the regime $r_c >> b$ the relaxation rate decreases as $T^{-3/2}$ as expected from the IR theory.[47] The expected dependence on magnetic field is also observed. At this time there is a factor of two uncertainty in the temperature scale at low temperatures and only approximate comparisons to theory have been made. However, the general shape of the experimental curve is not in doubt.

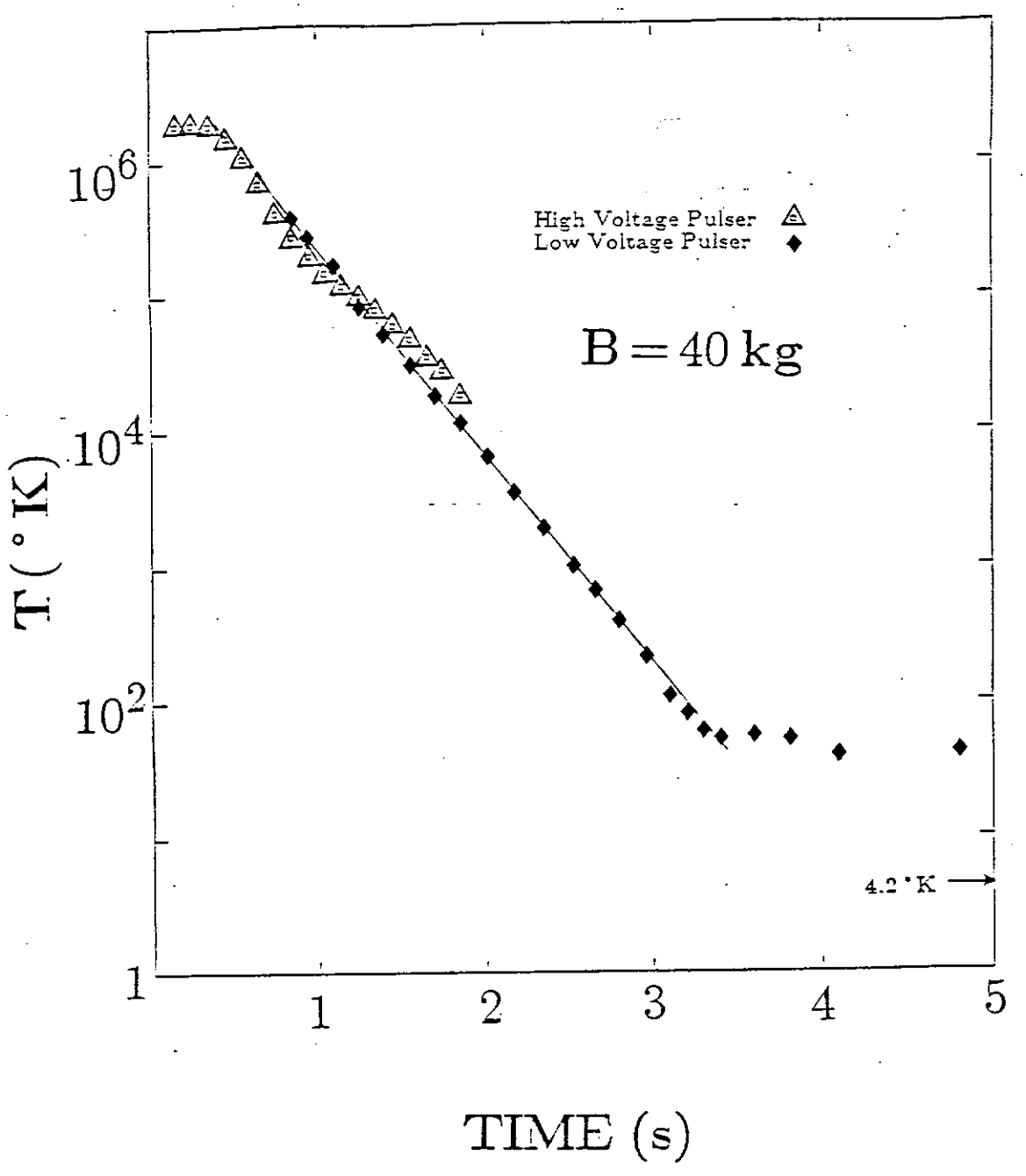

Figure 20. Plasma temperature vs. time.

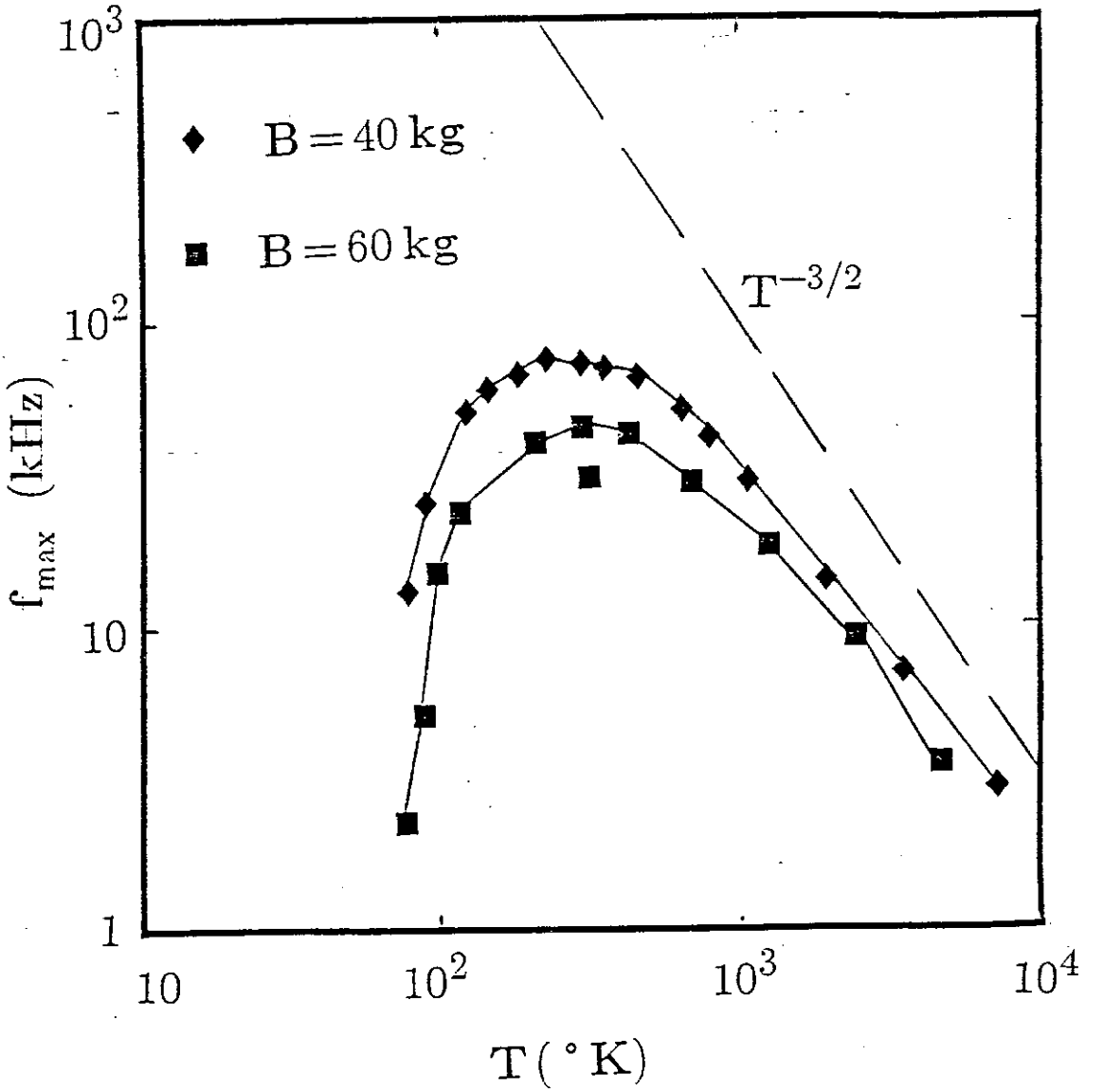

Figure 21. Modulation frequency for maximum heating vs. plasma temperature.

VII. SUMMARY

The results already obtained provide a convincing demonstration that the pure electron plasma can be used for a wide variety of experiments on waves, transport, and statistical mechanics. The experiments allow a gratifying precision and attractive simplicity unusual in plasma physics. A great many other experiments are possible with this system and a systematic understanding of the results from first principles is a reasonable goal.

ACKNOWLEDGMENT

This research was supported by ONR Contract N00014–82–K–0621; a series of NSF grants, currently PHY87–06358; and a series of Department of Energy grants, currently DE–FG03–85ER53199.

REFERENCES

1. J. H. Malmberg and J. S. deGrassie, Phys. Rev. Lett. **35**, 577 (1975).
2. C. F. Driscoll and J. H. Malmberg, Phys. Fluids **19**, 760 (1976).
3. J. H. Malmberg, "Electron Column from a Cathode with Radially Varying Potential," in preparation.
4. J. S. deGrassie and J. H. Malmberg, Phys. Fluids **23**, 63 (1980).
5. B. R. Beck, J. H. Malmberg and A. W. Hyatt, Bull. Am. Phys. Soc. **31**, 1391 (1986).
6. J. H. Malmberg and T. M. O'Neil, Phys. Rev. Lett. **39**, 1333 (1977).
7. J. H. Malmberg, T. M. O'Neil, A. W. Hyatt and C. F. Driscoll, Proc. of 1984 Sendai Symposium on Plasma Nonlinear Phenomena, 31 (1984).
8. A. W. Hyatt, C. F. Driscoll and J. H. Malmberg, Phys. Rev. Lett. **59**, 2975 (1987).
9. D. L. Eggleston, C. F. Driscoll, B. R. Beck, A. W. Hyatt and J. H. Malmberg, "Axial Energy Analyzer for Pure Electron Plasma Devices," in preparation.
10. T. Hsu and J. L. Hirshfeld, Rev. Sci. Instrum. **47**, 236 (1976).
11. J. S. deGrassie, Ph.D. Thesis, UCSD (1977).
12. R. C. Davidson, Theory of Nonneutral Plasmas (W. A. Benjamin, Reading, MA, 1974).
13. R. C. Davidson and N. A. Krall, Phys. Fluids **13**, 1543 (1970).
14. S. A. Prasad and T. M. O'Neil, Phys. Fluids **27**, 206 (1984).
15. C. A. Kapetanakos and A. W. Trivelpiece, J. Appl. Phys. **42**, 4841 (1971).

16. A. W. Trivelpiece and R. W. Gould, J. Appl. Phys. **30**, 1784 (1959).
17. J. H. Malmberg and C. B. Wharton, Phys. Rev. Lett. **17**, 175 (1966).
18. S. A. Prasad and T. M. O'Neil, Phys. Fluids **26**, 665 (1983).
19. W. Knauer, J. Appl. Phys. **37**, 602 (1966).
20. R. H. Levy, Phys. Fluids **8**, 1288 (1965).
21. C. A. Kapetanakos, D. A. Hammer, C. D. Striffler and R. C. Davidson, Phys. Rev. Lett. **30**, 1303 (1973).
22. R. J. Briggs, J. D. Daugherty, and R. H. Levy, Phys. Fluids **13**, 421 (1970).
23. W. D. White, J. H. Malmberg and C. F. Driscoll, Phys. Rev. Lett. **49**, 1822 (1982).
24. W. D. White and J. H. Malmberg, Bull. Am. Phys. Soc. **27**, 1031 (1982).
25. K. S. Fine, C. F. Driscoll and J. H. Malmberg, Bull. Am. Phys. Soc. **33** (Oct. 1988).
26. C. F. Driscoll, J. H. Malmberg and R. A. Smith, Bull. Am. Phys. Soc. **33** (Oct. 1988).
27. R. L. Kyhl and H. F. Webster, IRE Trans. Electron Devices **3**, 172 (1956).
28. C. A. Kapetanakos, D. A. Hammer, C. D. Striffler and R. C. Davidson, Phys. Rev. Lett. **30**, 1303 (1973).
29. G. Rosenthal, G. Dimonte and A. Y. Wong, Phys. Fluids **30**, 3257 (1987).
30. R. A. Smith, M. N. Rosenbluth, C. F. Driscoll and T. M. O'Neil, Bull. Am. Phys. Soc. **33** (Oct. 1988).
31. C. F. Driscoll, J. H. Malmberg, K. S. Fine, X-P. Huang and R. W. Gould in *Plasma Physics and Controlled Nuclear Fusion Research 1988*, Vienna: IAEA (1989); X-P. Huang, C. F. Driscoll and J. H. Malmberg, Bull. Am. Phys. Soc. **33** (Oct. 1988).
32. M. V. Melander, N. J. Zabusky and A. S. Styczek, J. Fluid Mech. **167**, 95 (1986).
33. M. H. Douglas and T. M. O'Neil, Phys. Fluids **21**, 920 (1978).
34. J. H. Malmberg and C. F. Driscoll, Phys. Rev. Lett. **44**, 654 (1980).
35. C. F. Driscoll and J. H. Malmberg, Phys. Rev. Lett. **50**, 167 (1983).
36. T. M. O'Neil, Phys. Fluids **23**, 2216 (1980).
37. C. F. Driscoll, K. S. Fine and J. H. Malmberg, Phys. Fluids **29**, 2015 (1986).
38. D. Wineland, et al., this conference.

39. D. L. Eggleston, T. M. O'Neil and J. H. Malmberg, Phys. Rev. Lett. **53**, 982 (1984).

40. D. L. Eggleston and J. H. Malmberg, Phys. Rev. Lett. **59**, 1675 (1987).

41. M. E. Rensink, et al., Physics Basis for MFTF-B (Lawrence Livermore Laboratory, Berkeley, CA, 1980); R. H. Cohen, et al., Nucl. Fusion **20**, 1421 (1980).

42. J. D. Crawford, T. M. O'Neil and J. H. Malmberg, Phys. Rev. Lett. **54**, 697 (1985).

43. J. D. Crawford and T. M. O'Neil, Phys. Fluids **30**, 2076 (1987).

44. C. F. Driscoll, J. H. Malmberg and K. S. Fine, Phys. Rev. Lett. **60**, 1290 (1988).

45. T. M. O'Neil and C. F. Driscoll, Phys. Fluids **22**, 266 (1979).

46. A. Simon, Phys. Rev. **100**, 1557 (1955).

47. C. L. Longmire and M. N. Rosenbluth, Phys. Rev. **103**, 507 (1956).

48. D. H. E. Dubin and T. M. O'Neil, Phys. Rev. Lett. **60**, 1286 (1988).

49. T. M. O'Neil, Phys. Rev. Lett. **55**, 943 (1985).

50. S. Ichimaru and M. N. Rosenbluth, Phys. Fluids **13**, 2778 (1970).

51. D. Montgomery, G. Joyce and L. Turner, Phys. Fluids **17**, 2201 (1974).

52. T. M. O'Neil and P. G. Hjorth, Phys. Fluids **28**, 3241 (1985).

53. P. G. Hjorth and T. M. O'Neil, Phys. Fluids **30**, 2613 (1987).

54. J. D. Lawson, The Physics of Charged-Particle Beams (Clarendon, NY, 1977), §3.3; Physica Scripta **T3** (1983).

55. B. R. Beck, Bull. Am. Phys. Soc. **33** (Oct. 1988).